DESIGN AND PERFORMANCE CHARACTERISTICS OF A MODELOCKED NEODYMIUM-GLASS LASER

by

RONALD MICHAEL NINNIS

B.Sc.(Honors)
University of British Columbia, 1969

A THESIS SUBMITTED IN PARTIAL FULFILLMENT OF
THE REQUIREMENTS FOR THE DEGREE OF
MASTER OF SCIENCE
in the Department
of
Physics

SIMON FRASER UNIVERSITY
June 1972

APPROVAL

Name: Ronald Michael Ninnis

Degree: Master of Science

Title of Thesis: Design and Performance Characteristics of a Modelocked Neodymium-Glass Laser

Examining Committee:

Chairman: J. F. Cochran

K. E. Rieckhoff
Senior Supervisor

J. C. Irwin

R. H. Enns

E. D. Crozier

Willis E. Lamb, Jr.
Professor of Physics
Yale University, U. S. A.

Date Approved: June 6/72

ABSTRACT

The design and operating characteristics of a Nd:glass pico-second laser facility are presented. A Brewster-cut laser rod is pumped by two linear Xenon flash-tubes within a double ellipse reflector configuration. Both the flash-tubes and laser rod are water-cooled for thermal stability. The optical cavity consists of a Fabrey-Perot resonator with an output mirror reflectivity of 65%. The laser was simultaneously Q-switched and passively mode-locked with a bleachable dye. The system is capable of producing a train of pulses, each pulse lasting 5×10^{-12} seconds with a power of 2×10^{9} watts. The pulse lengths are measured using a two-photon absorption technique. Several important effects associated with the pulse rate are reported and explained in terms of a theory of thermal lensing.

ACKNOWLEDGEMENTS

I am grateful to Dr. K.E. Rieckhoff for providing valuable advice and criticism extending well beyond the range of physical research. Dr. R. Menzel and Dr. R. Turner have stimulated many profitable discussions.

I am indebted to Mr. D.J. McMillan who initiated this project, completing a large part of the design. Also I appreciate the patience and hard work of Mrs Janice Inouye during the preparation of the manuscript.

Thank you, Val and Terry, for going through this with me.

TABLE OF CONTENTS

LIST OF FIGURES

For Gnossos and the Prince

Leaving us in between.

CHAPTER I

INTRODUCTION

"Maser techniques give the attractive promise of coherent amplification at the high (optical) frequencies and of generation of very monochromatic radiation" (Schawlow and Townes 1958). Since this conception, beginning with the ruby laser of Maiman (1960) and the helium-neon laser (Javan 1961) intensive research has been carried out to extend power capabilities of these devices. The aim was to develop a source of light with optical electric fields of sufficient strength to study the non-linear interaction of radiation with matter.

Solid state lasers by virtue of their high density of active ions are capable of producing coherent light pulses of extremely high intensity and short duration. The output of these lasers normally consists of random intensity fluctuations (spikes) during a period of $\sim$1 msec corresponding to the pump pulse duration.

Q-switching, a method of compressing part of the energy of this free emission into a short-lived, high power pulse, was proposed by Hellwarth (1961) and first realized by McClung and Hellwarth in 1962 using a Kerr cell. In this technique a fast optical switch is utilized to delay laser oscillation until near maximum population inversion is achieved, at which time the cavity losses are "switched off" resulting in a short (10^{-8} sec) burst of high intensity radiation. Peak powers of 10^{7} watts can be attained in this way. These pulses have found

application in such experimental investigations as optical harmonic generation (Franken and Ward 1963; Bloembergen 1965), stimulated Raman and Brillouin scattering (Chiao, Garmire and Townes 1964; Brewer and Rieckhoff 1964), optical parametric amplification (Giordmaine and Miller 1965), and were in fact the principal devices used for opening the field of "non-linear optics".

The second generation of short duration high intensity laser pulses resulted when the cavity longitudinal modes of a laser were locked in phase to form a repetitive pulse train within the Q-switched pulse envelope. This method involves modulating the cavity losses at the longitudinal mode separation frequency producing a definite phase relation between the oscillating modes. Linear superposition of these modes results in periodic constructive interference corresponding to a train of bandwidth-limited short pulses. Mode-locking has produced pico-second (10^{-12} sec) pulses having peak powers in the gigawatt (10^{9} watt) range.

Mode-locked pulse trains were first produced by Hargrove, Fork and Pollack (1964) using an ultrasonic diffraction modulator with a He-Ne gas laser. Other types of active modulators such as the K.D.P. Pockels-cells all have been used to mode-lock wider bandwidth lasers including neodymium glass and yttrium aluminum garnet (YAG) lasers.

In 1965 DeMaria, Stetser and Heynan found that certain bleachable dyes could act both as Q-switches and amplitude

modulators. Intensity modulation arises from the non-linear response of the absorber with a period equal to the cavity circulation time which naturally corresponds to the mode separation frequency as required for mode-locking. This method has the advantage that it is no longer necessary to make adjustments or depend on the stability of an external modulation circuit. Furthermore, the high non-linearity of the dye results in more high amplitude harmonics of the modulation and therefore narrower pulses (DeMaria 1968).

Neodymium glass lasers are especially suited for the generation of ultra-short pulses. Glass serves well as an optical host since it is simple to manufacture with excellent optical homogeneity and can withstand high peak powers. Impurity ions such as Nd^{3+} in glass find themselves in an environment of strong electric fields which Stark-split the complex ion multiplet structure resulting in a broad-band laser emission as well as an efficient pumping mechanism. The 100Å emission bandwidth of Nd:glass theoretically allows pulse widths in the 10^{-13} sec range.

However, one major disadvantage of using glass as the host material is its low thermal conductivity. The optical pumping requires intense flashes from broad-band arc-lamps; most of the energy in the flashes will appear as heat in the laser rod. With the sudden heating from each pump flash and the immediate cooling by water necessary for stable operation, thermal gradients and hence optical distortion will

inevitably occur in the laser rod.

A serious problem that arises in experiments with pico-second pulses is the frequency response limitation of the available electronic measuring apparatus. Consequently, a new technique has been developed in which the pulse length is obtained from an intensity correlation function displayed by non-linear optical processes, such as second harmonic generation (Armstrong 1967; Glenn and Brienza 1967). Two-photon absorption-fluorescence was first used for this purpose by Giordmaine et al. in 1967, and was employed here to investigate the pulse shape of the laser output when Q-switched and mode-locked.

This thesis describes the design and construction of a pico-second laser facility and reports on its performance characteristics. The important operating characteristics have been measured and the results discussed. Particular attention has been paid to the problem of thermal lensing and its many implications.

The theory of the Nd:glass laser, mode-locking, and pulse measurement techniques is presented in Chapter II. This is followed by a description of the design and construction of the laser facility in Chapter III. In Chapter IV the performance data are presented and discussed, including the effects of thermal lensing. The final Chapter provides a summary and suggests future developments.

CHAPTER II

THEORY

II-1 Neodymium:glass Lasers

The Nd:glass laser is a four-level solid state device. The lasing material consists of an active rare-earth ion dissolved into a silicate glass host. The excitation emission cycle involves four energy levels of the active ion rather than the three levels characteristic of the ruby laser. The lower state of the lasing transition is well above the ground state and is generally empty so that population inversion is more easily attained in comparison with the three-level system in which the ground state must be at least half-emptied before an inversion can be realized. This feature allows low threshold energies even at room temperature.

The electronic structures of the rare-earth elements start from the completed xenon configuration:

$$1S^2\ 2S^2\ 2P^6\ 3S^2\ 3P^6\ 3d^{10}\ 4S^2\ 4P^6\ 4d^{10}\ 5S^2\ 5P^6$$

Following cesium and barium which have one and two 6S electrons respectively, the rare-earth elements are built by adding to the vacant inner 4f and 5d states. Neodymium has four 4f electrons added to the barium structure. In its triply ionized state (Nd^{3+}) the two 6S electrons and one 4f electron have been removed. The lowest excited states occur when a 4f electron is promoted to an empty 4f or 5d state. This results in a

large number of possible states with nearly the same energy.

These excited states represent different combinations of orbital and spin angular momenta. The Russel-Saunders coupling scheme applies here so that the total angular momentum quantum number, J, represents the vector addition of the total spin and total orbital angular momentum of the three 4f electrons.

States with different combinations of angular momenta are split by coulomb repulsion. The lowest lying of these have their spins aligned (S = 3/2, 2S+1 = 4; quartets) and a total orbital angular momentum of L = 6. The possible J-values range from $|L+S| \rightarrow |L-S|$ and these states are split by spin-orbit coupling ($\Delta E \sim 2000$ cm^{-1}). They are designated $^4I_{9/2}$, $^4I_{11/2}$, $^4I_{13/2}$, $^4I_{15/2}$ where the superscript gives the spin multiplicity, the subscript is the J-value, and the letter I represents a total orbital momentum of 6 (I is the sixth letter in the series P,D,F,G,H,I,K,...).

Each of these J-states is 2J+1 degenerate corresponding to the various single component values of the total angular momentum. This multiplet structure is split by the Stark effect arising from the electric field of the host crystal or glass. These splittings are on the order of 100 cm^{-1}. It should be noted that each state must remain at least doubly degenerate in any electric field. This result appears in a well-known calculation by Kramers; hence Kramers doublets. Full details of these energy levels are presented in a paper by Mann and DeShazer (1970).

The lasing process involves transitions between the various angular momentum states. The usual selection rules are all lifted for these transitions due to mixing of states by associated spin-orbit coupling and the Stark electric field. For Nd:glass the useful transitions are from the $^4F_{3/2}$ level. Fluorescence at the wavelengths around 1.06 μ have various sublevels of the $^4I_{11/2}$ as its final state. Stimulated emission at longer wavelengths can occur with $^4F_{3/2} \rightarrow {}^4I_{13/2}$ (1.35 μ) while the $^4F_{3/2} \rightarrow {}^4I_{9/2}$ transition results in 0.914 μ radiation. The exact splitting of these levels depends on the nature of the host material. An energy level diagram for these useful transitions is shown in Fig. II-1.

The strongest fluorescence, $^4F_{3/2} \rightarrow {}^4I_{11/2}$, is the one normally used for glass lasers. The lower laser level being 2000 cm^{-1} above the ground state, there is negligible thermal population from the ground state since the occupancy, N_2, of the lower laser level relative to the population of the ground state, N_1, is given by the Boltzmann distribution

$$\frac{N_2}{g_2} = \frac{N_1}{g_1} e^{(E_1 - E_2)/kT}$$

where g_1 and g_2 are the respective degeneracies. Thus we have a four-level laser.

The upper state of the lasing transition is populated by non-radiative transitions from higher excited states which are themselves pumped from the ground state by the broad-band

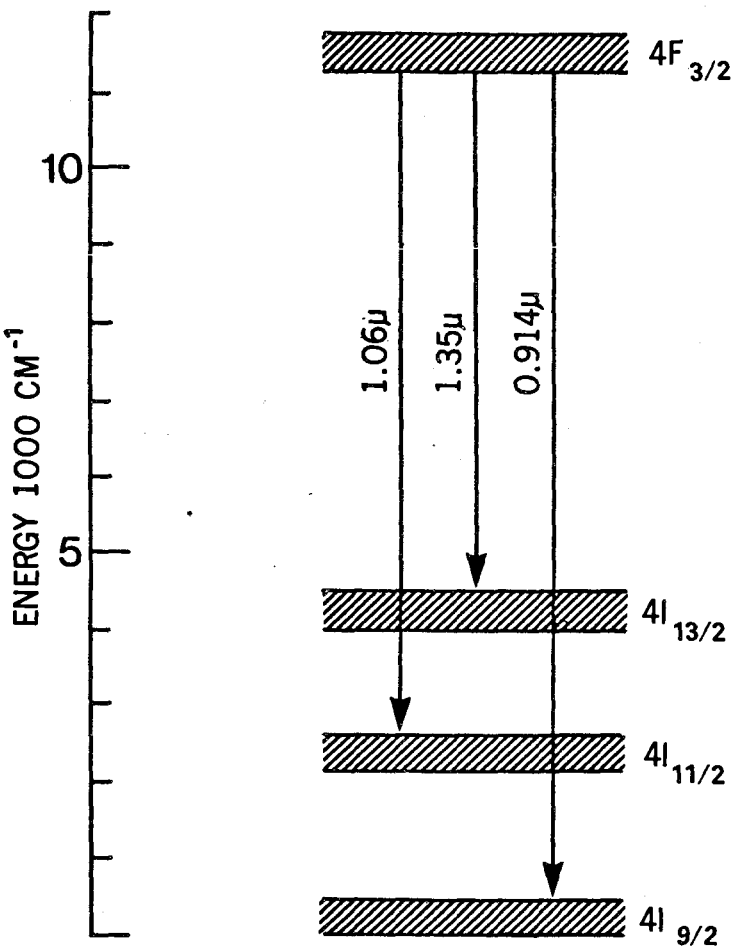

FIG II-1

ENERGY LEVEL DIAGRAM FOR NEODYMIUM IN GLASS WITH LASING TRANSITIONS SHOWN. EACH LEVEL REPRESENTS A GROUP OF CLOSELY SPACED LINES

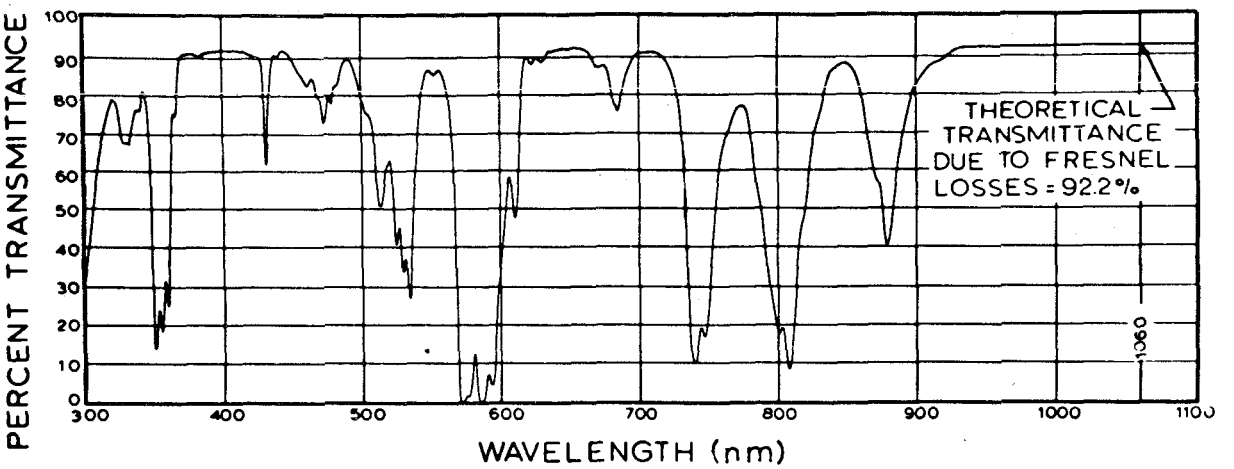

Nd^{3+} absorption spectrum for a 6.4 mm thick sample of a glass with the composition 66 wt.% SiO_2, 5 Nd_2O_3, 16 Na_2O, 5 BaO, 2 Al_2O_3, and 1 Sb_2O_3. After R.D. Maurer.

FIG II - 2 TYPICAL ABSORPTION SPECTRUM FOR Nd^{3+} DOPED GLASS

radiation from xenon flash-tubes. Fig. II-2 is the absorption spectrum for neodymium in glass. The largest absorption line is around 5800A and corresponds to transitions from ground state to the $^2G_{7/2}$ and $^4G_{5/2}$ levels. The low optical density at these wavelengths is due to the many levels available with the host Stark splitting of the degenerate J-states. Consequently the important component of the pump light spectrum corresponds to the centre of the visible region.

The laser emission is broadened by several mechanisms (Snitzer 1966). The emission starts at a single Kramers doublet of the $^4F_{3/2}$ level and terminates at a level which must consist of several overlapping Kramer's doublets in the Stark split, $^4I_{11/2}$ state. The emission would therefore be expected to consist of several overlapping unresolved lines. In addition to this splitting, inhomogeneous broadening occurs as a result of the variations in the host sites for the Nd^{3+} ions. Also there is homogeneous broadening due to thermal broadening of the ion emission.

Fig. II-3 shows the energy level scheme of a four-level laser. Level 1 is the ground state, level 4 corresponds to the various upper excited states and 3→2 is the laser transition. The W's, A's, and S's refer to the stimulated, spontaneous, and non-radiative transition rates respectively.

A rigorous description of the kinetics of a four-level laser (Steele 1968) involves transitions to and from all four

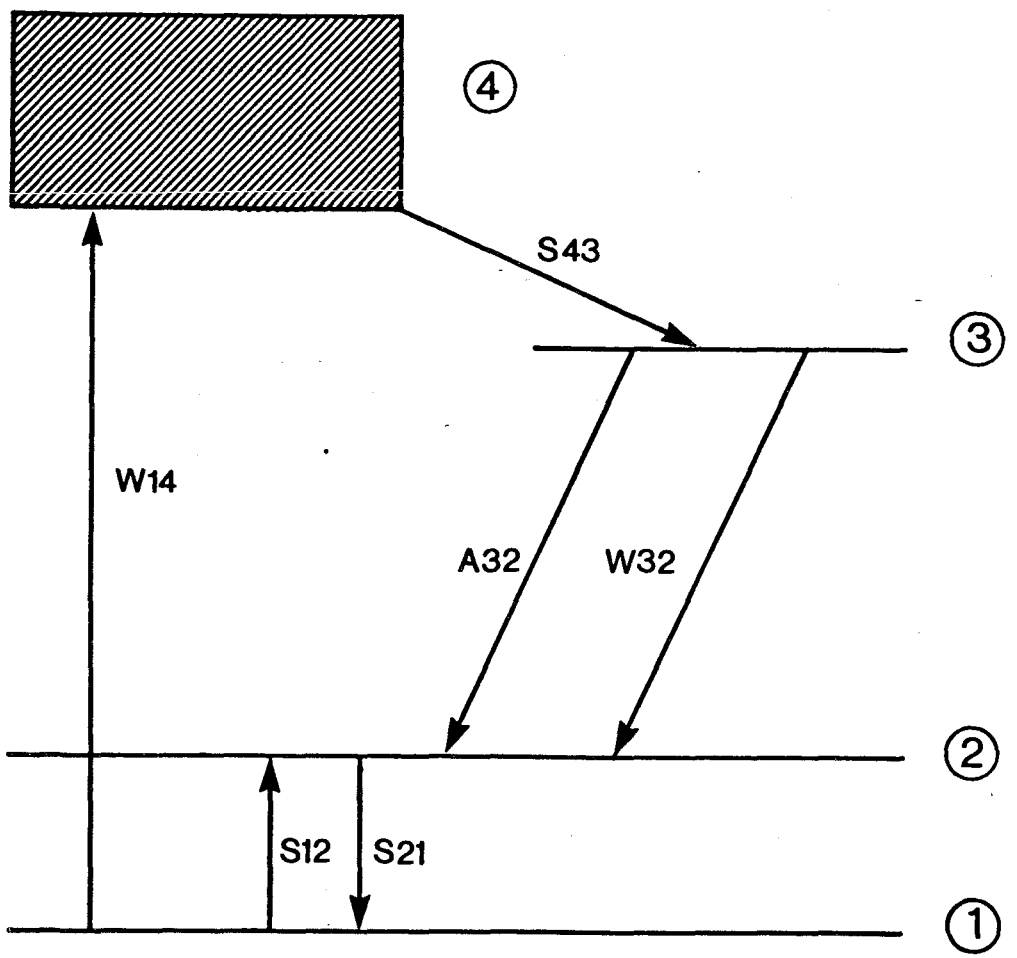

FIG II-3
ENERGY LEVEL DIAGRAM FOR A FOUR – LEVEL LASER

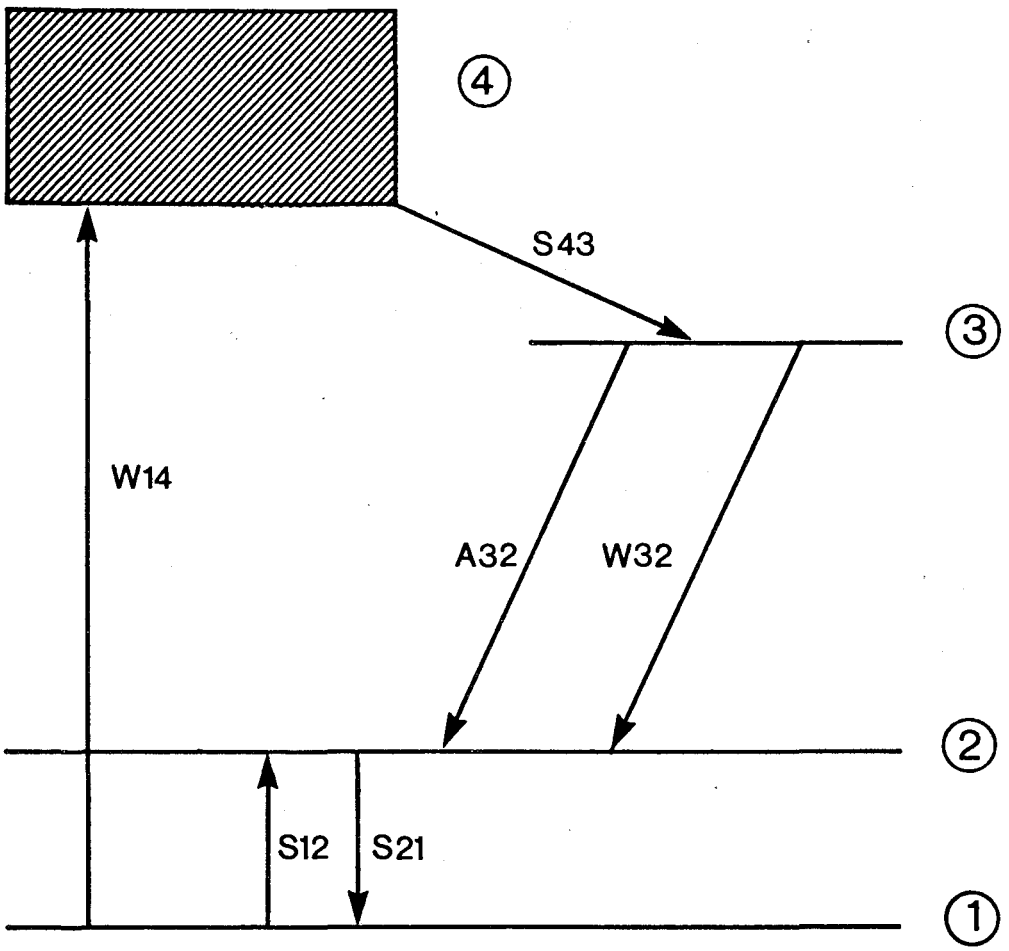

FIG II-3
ENERGY LEVEL DIAGRAM FOR A FOUR – LEVEL LASER

states along with their population densities. However, by ignoring the very fast transition rates we can examine in a very simple manner (following Lengyel) the features of a laser such as Nd:glass.

We first assume that the non-radiative rates are so fast that the upper laser state is populated directly from the ground level. Further, we consider S_{12} and S_{21} to be so fast ($S_{21}^{-1} \sim 10^{-7}$ sec) that level 1 and level 2 are in thermal equilibrium and thus populated according to the Boltzmann distribution as in equation (1). Since $E_2-E_1 \sim 2000$ cm^{-1} and kT ~ 200 cm^{-1} at room temperature, level 2 is always essentially empty. Finally we note that the transition 3→1 is forbidden and the spontaneous rate 3→2 is slow ($\sim$1 msec for Nd:glass).

With these assumptions we can ignore the populations of levels 2 and 4 and we have approximately a two-level laser. Then the rate equation governing the population density N_3 of the upper laser level before oscillation is simply

$$\frac{dN_3}{dt} = W_{14} N_1 - A_{32} N_3 \qquad (2)$$

For the steady state condition, $\frac{dN_3}{dt} = 0$, we have

$$W_{14} N_1 = A_{32} N_3 \qquad (3)$$

The Schawlow-Townes expression for the critical population inversion required for oscillation is

$$\Delta N_c \equiv \left(N_3 - N_2 \frac{g_3}{g_2}\right)_c = \frac{8\pi \nu^2 t_s}{c^3 t_p g(0)} \qquad (4)$$

In this expression, g_2 and g_3 are the respective level degeneracies, ν is the frequency of the oscillating mode, i.e. near the center of the laser transition, $t_s = A_{32}^{-1}$ is the spontaneous life-time of the upper laser state and $g(0)^{-1} \sim \Delta\nu$, the transition line-width. Equation (4) is obtained by requiring that the gain of the medium (expressed in terms of the population inversion) be equal to the total losses of the optical cavity. The losses are primarily reflection losses and are characterized by the average life-time, t_p, of a photon in the resonator. The photon life-time can be related to the Q-factor of the cavity by the formula

$$Q = 2\pi \nu t_p \qquad (5)$$

The power input can be expressed in terms of the pump photon energy, $h\nu_p$, and the volume, V, of the active medium as

$$P = h\nu_p W_{14} N_1 V = h\nu_p A_{32} N_3 V \qquad (6)$$

using equation (3).

Since we have assumed level 2 to be empty, N_3 is given by equation (4) with $N_2 = 0$ and substitution into equation (6) yields the threshold power input

$$P_T = \frac{8\pi\nu^2 \Delta\nu\, h\nu_p V}{c^3 t_p} \qquad (7)$$

The threshold power does not depend on the exact life-time of the upper laser state but does increase with the lasing transition bandwidth, $\Delta\nu$. The presence of ν^2 in this expression points out one of the difficulties in obtaining maser action in the optical regions in comparison with the microwave frequencies.

II-2 Mode-Locking: General

Longitudinal modes of an optical resonator correspond to allowed standing wave patterns so that integral numbers of half-wavelengths must fit between the mirrors, i.e.

$$m\frac{\lambda}{2} = L_{opt} \tag{1}$$

where L_{opt} is the optical path length of the cavity. Thus there are a sequence of allowed cavity resonances, ν_m, separated by equal frequency intervals

$$\Delta\nu \equiv (\nu_m - \nu_{m-1}) = \frac{c}{2L_{opt}}. \tag{2}$$

Those modes which lie within the laser's gain bandwidth, $\Delta\lambda$, as determined by the atomic resonances of the laser material and frequency selective losses are allowed to oscillate. The number of allowed longitudinal modes is then

$$n = \frac{2L_{opt}\,\Delta\lambda}{\lambda^2} \tag{3}$$

where λ is the emission wavelength. For typical Nd:glass lasers, $L_{opt} \sim 1$ m, $\Delta\lambda \sim 100$Å, $\lambda = 1\ \mu$, so we have $n \approx 5000$. See Fig. II-4.

Mode-locking refers to the amplitude and phase coupling of these modes to form a repetitive pulse train. The correct description of this process and its observable implications

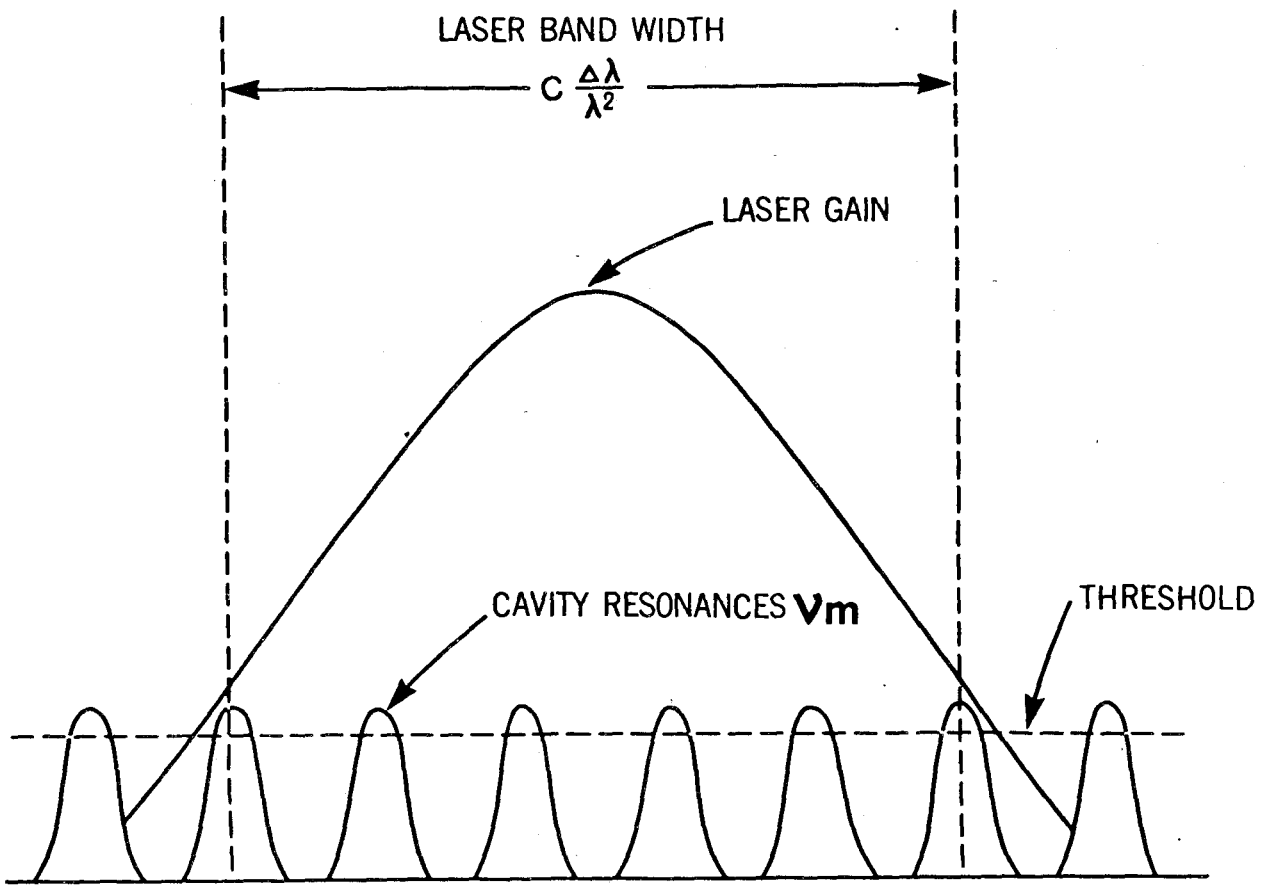

FIG II-4
RESONATOR PROFILES

are still very much a matter of debate. However, the main features can be understood in terms of a simple model involving amplitude modulation of the cavity electric fields.

If we assume a single mode, ν_0, oscillates first and then is amplitude modulated (for example, by varying the cavity losses) at a frequency equal to the mode separation, side-bands will appear at the adjacent modes. These modes will be induced to oscillate in phase with the original signal and in turn generate more side-bands, the process continuing up to the bandwidth of the laser. The phase-locking means that at some time, say t = 0, the modes will all be in phase so for n modes we can write the total field as the sum:

$$E(t) = \sum_{a=-\frac{1}{2}(n-1)}^{\frac{1}{2}(n-1)} e^{i(\omega_0 + a\Delta\omega)t} \tag{4}$$

$$= e^{i\omega_0 t} \sum_{a=-\frac{1}{2}(n-1)}^{\frac{1}{2}(n-1)} e^{ia\Delta\omega t}$$

$$= e^{i\omega_0 t} \frac{2\sin\left(\frac{n\Delta\omega}{2}t\right)\sin\left(\frac{\Delta\omega}{2}t\right)}{1-\cos(\Delta\omega t)}$$

$$= e^{i\omega_0 t} G_n(t)$$

where we have assumed equal amplitudes of unit height. The term $G_n(t)$ is identified as the envelope function over the carrier frequency, ω_0. Fig. II-5 shows $G_n(t)$ plotted for five equal amplitude modes.

Equation (4) reveals several interesting results of mode-locking. First of all, as n becomes large, $G_n(t)$ approaches the form of a pulse train of period $T = \frac{2\pi}{\Delta\omega} = \frac{2L_{opt}}{c}$, i.e. the time required for a pulse to complete a cavity round trip. The pulses are separated in space by twice the cavity length.

Also, the pulse width is seen to be approximately $\tau \cong \frac{2\pi}{n\Delta\omega} = I$. Using equation (3) for the number of allowed modes, n, we find $\tau \cong \frac{\lambda^2}{c\Delta\lambda} = \frac{1}{\Delta\nu}$. This important result shows that the pulse shortening is limited by the required harmonic content and hence the natural linear width of the laser transition. For Nd:glass we have typically $\Delta\lambda = 100\text{Å}$ and $\tau_{min} = 3 \times 10^{-13}$ sec.

Finally, if we assume equal amplitude modes, then the peak field amplitude, A_F, which occurs each time themmodes align in phase is just n times the single mode amplitude. Also the peak power is n times the power of randomly phased modes.

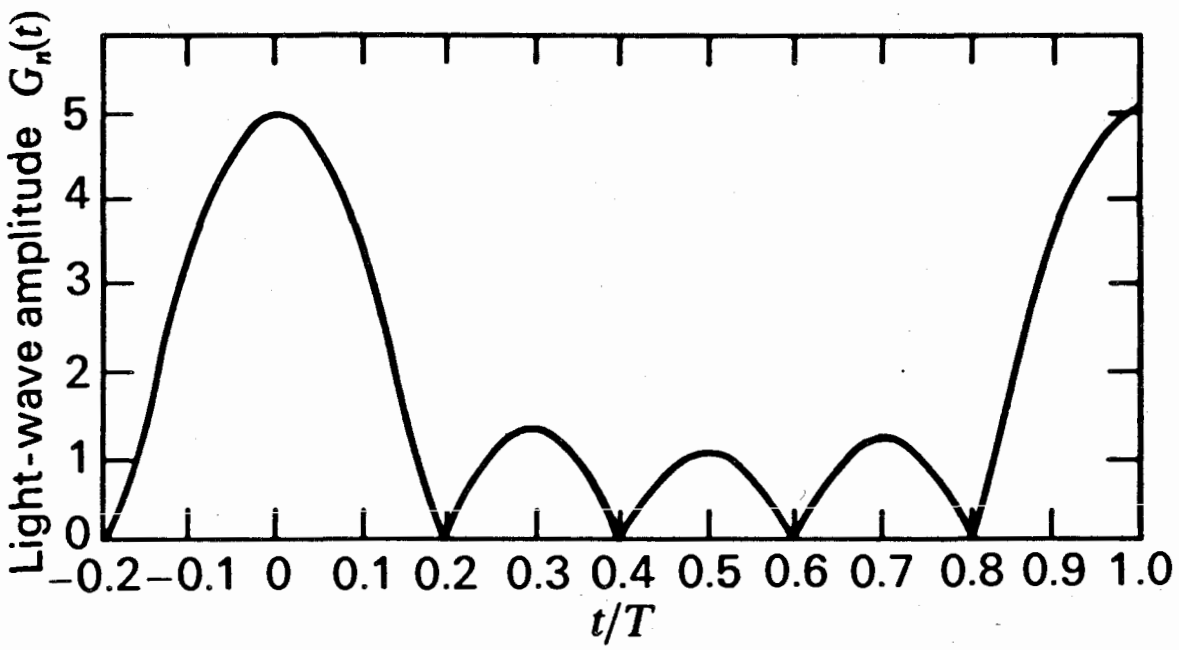

A plot of one period of the optical envelope function $|G_n(t)|$ resulting from phase locking of five (n= 5) equal-amplitude waves of frequency spacing T^{-1} by "loss" modulation.

FIG II-5 Gn(t) FOR FIVE EQUAL AMPLITUDE MODES

II-3 Mode-Locking: Passive

As shown above, mode-locking requires some method of modulating the cavity losses at the longitudinal mode separation frequency. Active modulation has been achieved with ultrasonic diffraction cells and K-D-P Pockels-cells. These methods are preferred when a continuous train of very stable pulses at high repetition rates is required.

In passive Q-switching by means of saturable absorption, the bleachable dye introduces an intensity dependent absorption into the cavity (see Fig. II-6). The laser is not allowed to oscillate until the fluorescent intensity reaches a critical value, I_0, corresponding to the saturation of the dye transition. The subsequent bleaching of the absorber and sudden increase in resonator Q results in the dumping of a large population inversion in a very short time. This technique applied to ruby and neodymium lasers can result in megawatt peak powers and pulse durations of the order of 10^{-8} sec.

The non-linearity of the bleachable dye can be employed as an intrinsic amplitude modulator, thus achieving simultaneously Q-switching and mode-locking. When two or more modes begin oscillating, their mutual interference causes a periodic amplitude fluctuation at the difference frequency, $\Delta\nu$. This initially sinusoidal waveform becomes distorted, the peak to peak variation being enhanced after passage through the non-linear absorber. With this sharpening of the amplitude distribution additional side-bands are added to the frequency

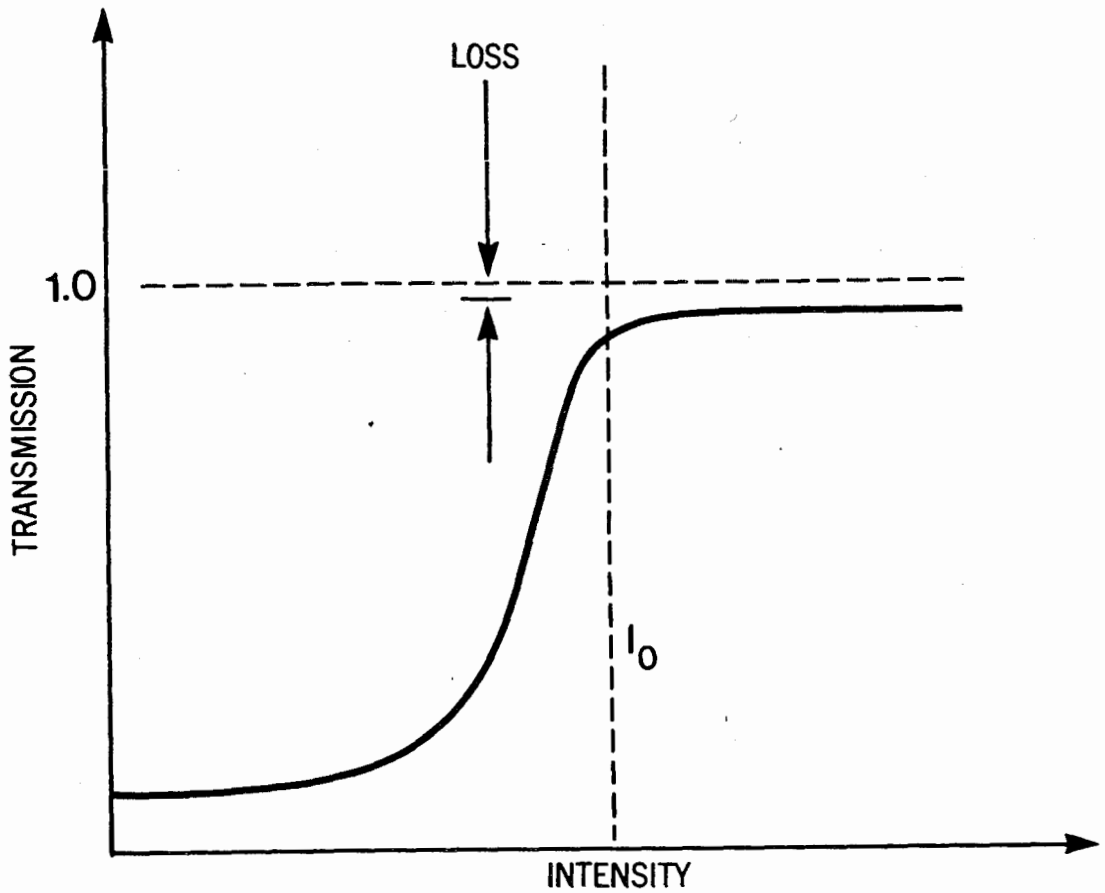

FIG II-6
NON-LINEAR TRANSMISSION OF A SATURABLE ABSORBER
USED IN Q-SWITCHING

spectrum. Since these side-bands represent other modes oscillating with a definite phase relationship, the result is passive mode-locking with all the aforementioned implications.

The theory of passive mode-locking originated with Cutler's (1954) description of the microwave regenerative pulse generator. Yariv (1965) has calculated mode-locking effects by introducing a time dependent conductivity loss factor into Maxwell's equations in a normal-mode expansion of the cavity radiation field. J.A. Fleck, Jr. (1968) analyzed passive mode-locking in terms of travelling waves, showing the essential equivalence to the normal-mode expansion descriptions.

Yariv points out that the field configuration represented by a mode-locked pulse train is favoured by a non-linear absorber over all other possibilities. This is because this configuration represents the highest energy density and will consequently suffer, for a given stored energy, the least loss in the non-linear absorber. A higher energy density is disallowed by bandwidth limitations.

The properties thus required of a dye solution for passive mode-locking are that it has

1. an absorbing transition at the laser frequency,
2. a bandwidth greater than or equal to the laser line width, and
3. a recovery time shorter than the cavity circulation time.

II-4 Theory: Measurement of Pulse-Structure

The usual method of measuring optical pulse lengths with a fast photodetector and travelling wave oscilloscope does not suffice for the pico-second regime. The shortest rise-time attainable with this method is $\sim$1/3 nanosecond, which implies that a pico-second pulse-train will be displayed in an integrated form. Linear correlation techniques such as Michelson interferometry and measurement of the power density spectrum can be shown (DeMaria 1969) to provide information regarding only a lower limit to the time duration of a pulse. In order to determine the actual length of the pulse, it is necessary to observe a non-linear response to the optical signal which gives a measure of the auto-correlation of the pulse intensity rather than the pulse amplitude.

The simplest technique takes advantage of the non-linearity of a two-photon absorption process to provide this information. Although any non-linear response will do in principle the usual methods involve some elaboration of second harmonic generation or two-photon absorption. For completeness we have presented in Appendix A a quantum mechanical calculation of the two-photon absorption process used in this work. The essential result is that the two-photon fluorescence (T.P.F.) intensity, I_f, is proportional to the square of the input intensity, I_0; $I_f \propto I_0^2$.

Suppose two pulses separated by a time, τ, are passed through an absorption-fluorescence cell. The first pulse is reflected back to collide with the second pulse at a distance

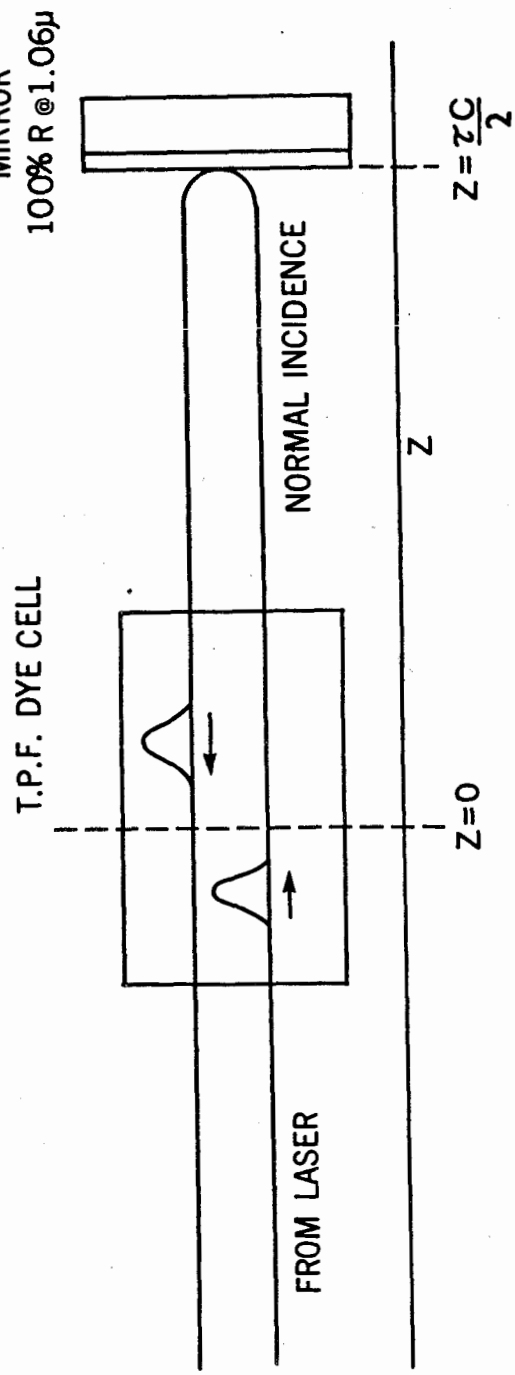

FIG II-7

SCHEMATIC OF TPF CORRELATION EXPERIMENT

$z = \frac{\tau c}{2}$ from the mirror (see Fig. II-7). A camera situated around z = 0 will then record the spatial dependence of the integrated power. Clearly, if the absorption was linear so that the fluorescence power was proportional to the input intensity, the film would record a uniform trace with no spatial variation. With a non-linear response, however, the coincidence of the pulses in space and time (i.e. collisions) would produce more fluorescence than both acting separately. Thus the film would record bright spots on a uniform background that would correspond to the spatial convolution of the two pulses and so afford a measure of their length.

Suppose (following DeMaria 1969) we write the oncoming pulse and reflected pulse as

$$E_1 = E_1(t - z/c)\, e^{i(kz - \omega t)} \quad \text{and} \quad E_2 = E_2(t + z/c)\, e^{i(-kz - \omega t)}$$

(E_1+E_2) are the envelopes representing the modulation of the carrier frequency, ω. The intensity of the sum of these waves is just

$$I_\omega = (E_1 + E_2)(E_1 + E_2)^*$$

$$= E_1^2(t - z/c) + 2\, E_1(t - z/c)\, E_2(t + z/c) \cos 2kz + E_2^2(t + z/c)$$

Since the fluorescent intensity is proportional to I_ω^2,

$$I_f \sim I_\omega^2 = E_1^4(t-z/c) + E_2^4(t+z/c) + 2E_1^2(t-z/c)E_2^2(t+z/c)$$
$$\times [1 + 2(\cos 2kz)^2] + 4[E_1^3(t-z/c)E_2(t+z/c)$$
$$+ E_1(t-z/c)E_2^3(t+z/c)]\cos 2kz .$$

The limited resolution of the film corresponds to taking a spatial average over several wavelengths so we can write

$$\langle(\cos 2kz)^2\rangle = \frac{1}{2} \quad \text{and} \quad \langle \cos 2kz \rangle = 0$$

Finally, integrating over all time gives the total film exposure as

$$S(z) = \int_{-\infty}^{\infty} E_1^4(t-z/c)\,dt + \int_{-\infty}^{\infty} E_2^4(t+z/c) + 4\int_{-\infty}^{\infty} E_1^2(t-z/c)E_2^2(t+z/c)\,dt$$
$$+ 4\int_{-\infty}^{\infty} E_1^2(t-z/c)E_2^2(t+z/c)\,dt .$$

For the case of equal amplitudes, $E_1 = E_2$, we have

$$S(z) = 2\int_{-\infty}^{\infty} E^4(t)\,dt + 4\int_{-\infty}^{\infty} E^2(t-z/c)E^2(t+z/c)\,dt .$$

Writing $\tau = \frac{2z}{c}$, the time between the pulses, we have

$$\frac{S(\tau)}{W} = 1 + 2G(\tau)$$

where the normalization factor

$$W = 2\int_{-\infty}^{\infty} E^4(t)\,dt$$

gives the background intensity and

$$G(\tau) = \frac{\int_{-\infty}^{\infty} E^2(t)\, E^2(t-\tau)\,dt}{\int_{-\infty}^{\infty} E^4(t)\,dt}$$

is the intensity correlation function or Glauber's second-order coherence function.

At $\tau = 0$ (where the pulses collide), $G(\tau) = 1$ and we have a peak normalized response of

$$\frac{S_{peak}}{W} = 3 .$$

While, when τ is large enough so that no overlap exists, $G(\tau) = 0$ and

$$\frac{S_{background}}{W} = 1 .$$

The contrast ratio of the film exposure for bandwidth limited short pulses is therefore 3:1. The resulting bright region of the photographic film represents the spatial convolution of the pulses thus giving a measure of their length.

The importance of the contrast ratio in this sort of measurement has been pointed out by Weber and Dändliker (1968).

They have shown that the contrast ratio for a thermal or Gaussian source of light with bandwidth $\Delta\nu$ is R = 1.5. Since a free-running laser with a large number of randomly phased modes corresponds to a Gaussian source, the absence of mode-locking results in the same spatial pattern of fluorescence but with a contrast ratio of 1.5:1. Thus the contrast ratio in this measurement is a necessary feature for distinguishing the mode-locked conditions.

Experimental results usually have the contrast ratio between 2 and 3. In an effort to explain this, Picard and Schweitzer (1970) give a detailed analysis of this correlation technique and have calculated the fluorescence patterns expected for two interesting models of mode-locking. In the partial-locking model, it is assumed that only those modes near the center of the laser gain profile are locked and the remainder are randomly phased. The contrast ratio for T.P.F. varies monotonically between R = 3 and R = 1.5 with the number of locked modes. Also an easily observable background signal is predicted for fast detector-oscilloscope displays. The domain model, on the other hand, assumes that mode-locking occurs within discrete sets domains of axial modes, the sets having random relative phase and extending across the whole of the laser spectrum. In this case the analysis again gives variable contrast ratio according to the number of independent domains. The domain model predicts a fine structure in the T.P.F. trace but does not demand background signals in photodetector-

oscilloscope displays.

The domain model is supported by the observed infinite contrast ratios in photo-diode-oscilloscope measurements and the results of Shapiro and Duguay (1969) in their measurements of the structure of the T.P.F. profile.

CHAPTER III

DESIGN AND CONSTRUCTION

III-1 Design

The basic requirements in the overall design of a picosecond facility are efficiency, stability and long term reliability. The laser head is designed to most effectively convert the available pump power to useful output. The flashtubes and active medium are water-cooled and temperature controlled. The structural details are designed for strength and flexibility.

There are three basic elements in a laser system. The active medium, in this case a suitably doped glass rod, provides the optical gain. The population inversion for this amplification is obtained by optical pumping with linear flashtubes. The regenerative feedback for oscillation is the function of the optical cavity which consists of two mirrors aligned normal to the optic axis of the amplifier. These elements are described separately below.

III-2 Active Medium

The active medium consists of a high quality glass host into which has been dissolved Nd^{3+} ions. Since the medium is solid, a high density of active ions is feasible resulting in a much higher gain per unit length than could be obtained with gas lasers. The host material is a borosilicate glass of a highly homogeneous composition. The doping was 3% (by weight Nd_2O_3).

The rods were 20.5 cm long and 1.0 cm in diameter. The ends were cut in a Brewster-Brewster configuration, parallel to within 5 sec of arc, and polished flat to within 1/10 λ_{Na}. The Brewster angle refraction results in the laser emission being polarized in the plane in which the reflection losses are minimized. Reflection from surfaces internal to the cavity should be avoided for mode-locking operation where a single well-defined feedback length is required. The rods were roughened on the surface to avoid specular internal reflection.

The rods were not cut exactly at the Brewster angle given by

$$\alpha = \tan^{-1} n = 57°16'$$

where n is the index of refraction. They were cut instead at the angle 54° so as to fix the laser output at the convenient angle of 30° with respect to the optic axis. The resulting

reflective loss is less than 1%.

Two (commercially available) rods were used: one an Owens-Illinois ED-2 glass and the other a Schott LG56 glass. The latter product is designed to have a small temperature coefficient of the index of refraction to minimize thermal distortion which can accompany pumping.

III-3 Resonator

The resonant cavity consisted of a pair of dielectric mirrors aligned normal to the rod's optic axis (see Fig. III-1(a)). These mirrors must withstand the very high peak powers produced with mode-locking ($\sim 10^9$ watts/cm^2). The mirrors were manufactured by Valpey Corp. using fused silica polished to a surface figure of 1/10 λ_{Na} on both sides. One mirror was 100% reflecting at 1.06 μ while the exit mirrors had a reflectivity of 65%. The exit mirror was wedge-shaped with an angle $\geq \frac{1}{2}^\circ$ from plane-parallel so as to eliminate feedback from the uncoated surface. The front mirror can easily be moved to change the cavity length as desired. The cavity length was usually about 1 meter.

Fig. III-1(b) shows the geometry of the optical cavity. The usual line-up procedure is complicated by the wedge shape of the exit mirror.

The alignment procedure used was as follows. The front mirror is first rotated so that the wedge angle lies in the vertical plane as shown so that horizontal adjustment does not affect transmitted rays. (Note that the wedge-shaped mirror now bends the beam slightly in the vertical plane.) A helium-neon line-up laser is then passed through a pin-hole which is situated $\sim$2m from the cavity. The He-Ne output is aligned at 30° to the rod axis and in the horizontal plane. The front mirror is then aligned by bringing the reflection from the coated surface into coincidence with the pin-hole. The front

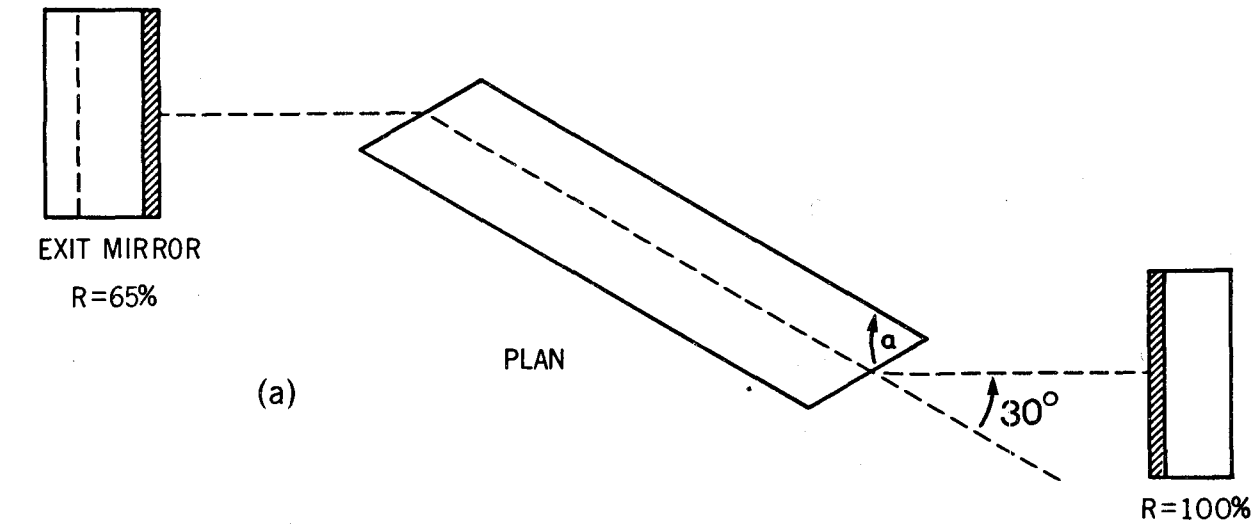

(a)

(b)

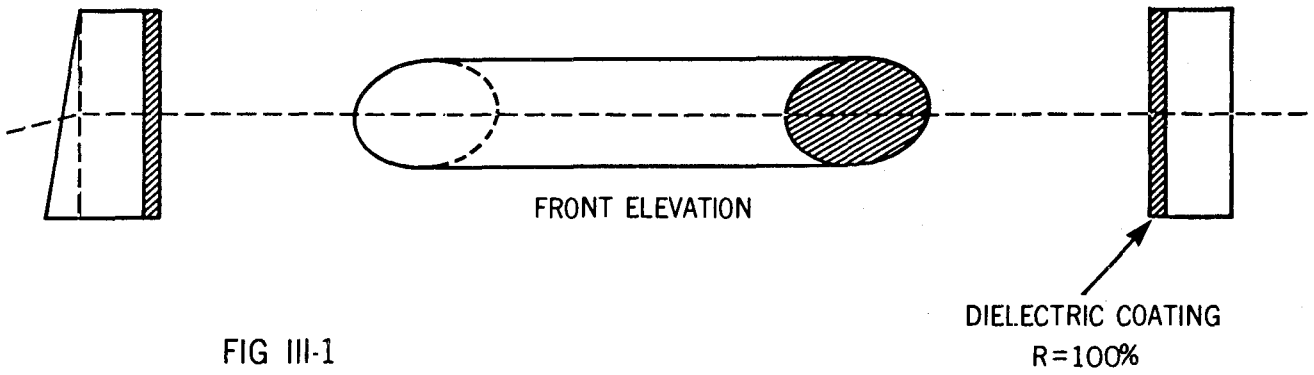

FIG III-1
OPTICAL RESONATOR

mirror can now be rotated in the horizontal plane allowing the fainter reflection from the back mirror (R = 100%) to be positioned over the pin-hole. Finally the front mirror is realigned horizontally.

This procedure is accurate enough to allow lasing. The alignment can be optimized by fine adjustment to the front mirror while observing the size and shape of the beam pattern on a developed, unexposed Polaroid film.

III-4 Optical Pumping

The rod was optically pumped over the whole visible spectrum by two linear xenon flash-tubes EG + G - FX45C-6. These tubes each have a maximum input energy of 2000 joules with an arc length of 6 inches. The minimum operating voltage of ∿20 kV is required to initialize the discharge. A typical flash duration is 1.4 msec as controlled by the power supply inductance.

The power was supplied from a bank of 8 - 100 μfarad - 2000 volt condensers which are designed to store a maximum of 1600 joules. (Occasionally the condensers were charged up to 2500 volts or 2500 joules.) Fig. III-2 is a circuit diagram for the pumping system. The 850 μH inductance along with the arc resistance of 0.6 Ω determines the pulse duration and shape. Fig. III-4 shows the flash intensity interchange as a function of time, as measured with a 925 photo-diode. The pulse duration was consistently 1.4 msec.

Fig. III-3 shows the circuit diagram of the trigger and automatic trigger. The timer pulse output occurs at a repetition rate governed by the time constant of the emitter circuit. When C_1 reaches a critical voltage, the emitter-base diode is forward biased and C_1 is discharged across R_1. This pulse is used to fire the SCR of the trigger circuit, discharging C_2 through the primary of the ignition coil. The output voltage appearing across the load inductance is limited by the breakdown of the adjustable spark gap. This system supplies a 25 kV pulse to the laser head resulting in sufficient electric

field gradient to initiate breakdown within the xenon flash-tubes.

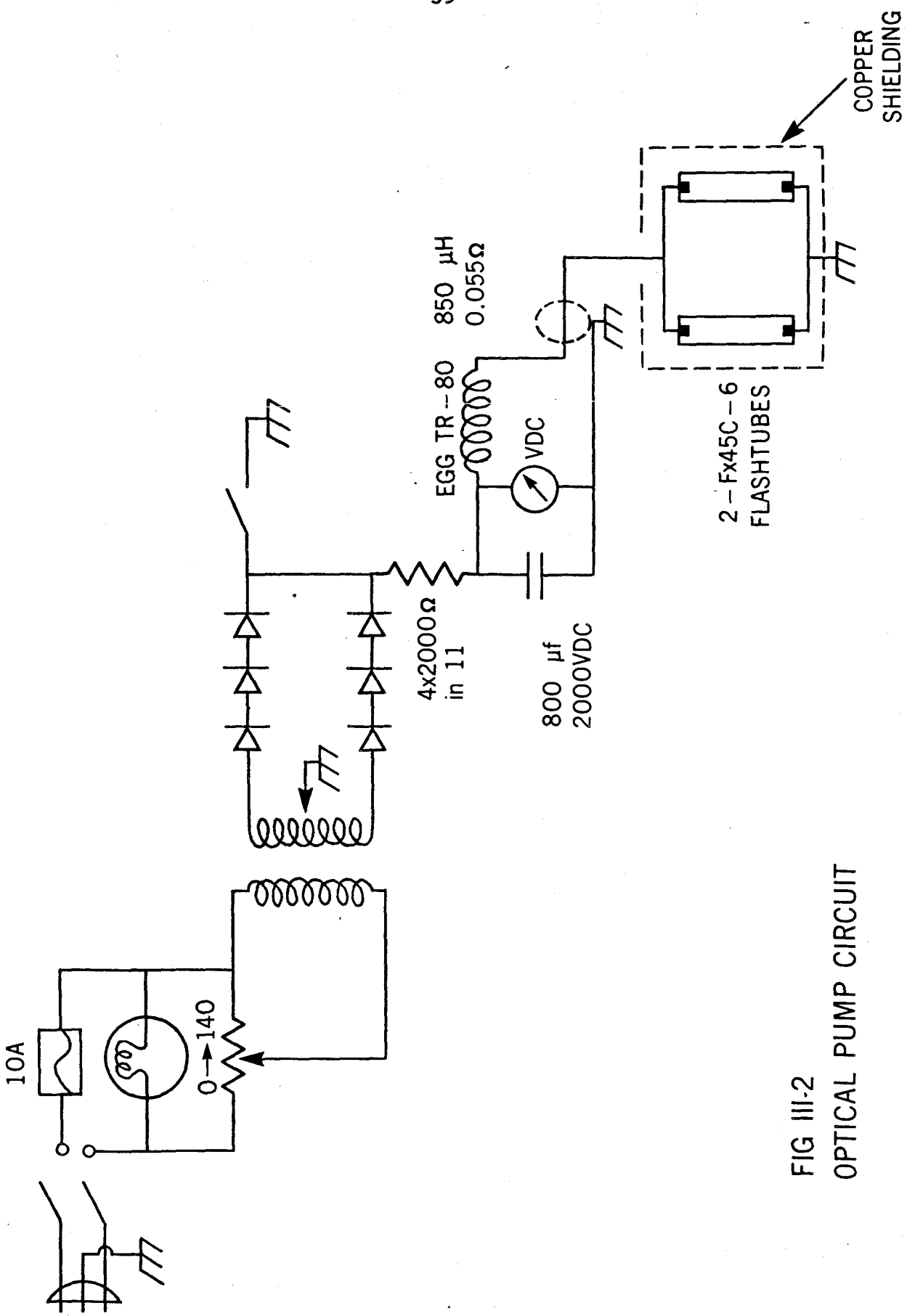

FIG III-2
OPTICAL PUMP CIRCUIT

TRIGGER

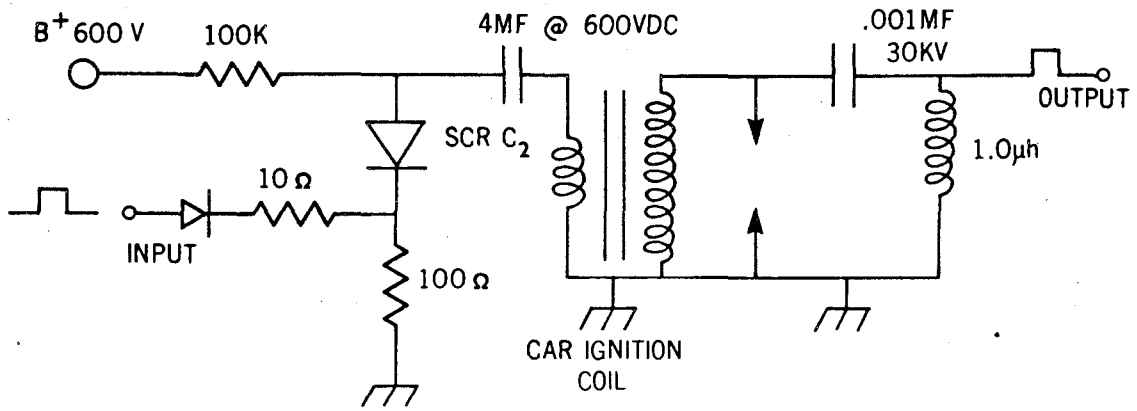

TIMER

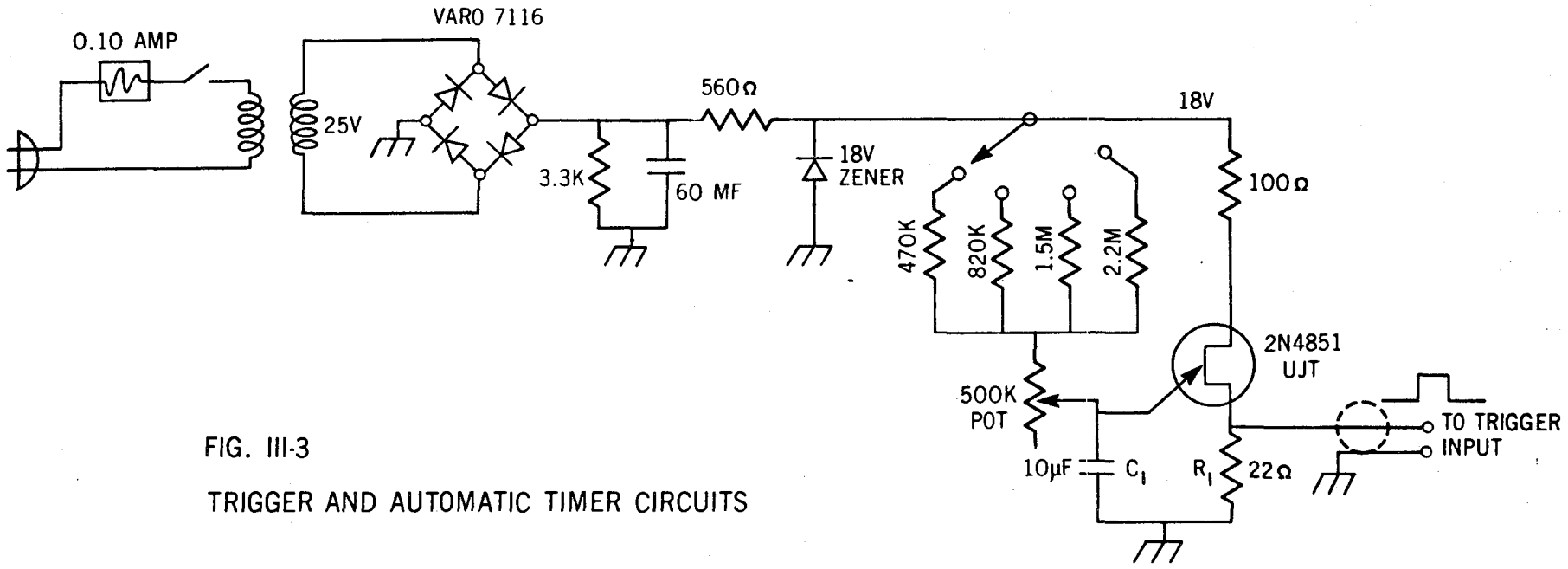

FIG. III-3

TRIGGER AND AUTOMATIC TIMER CIRCUITS

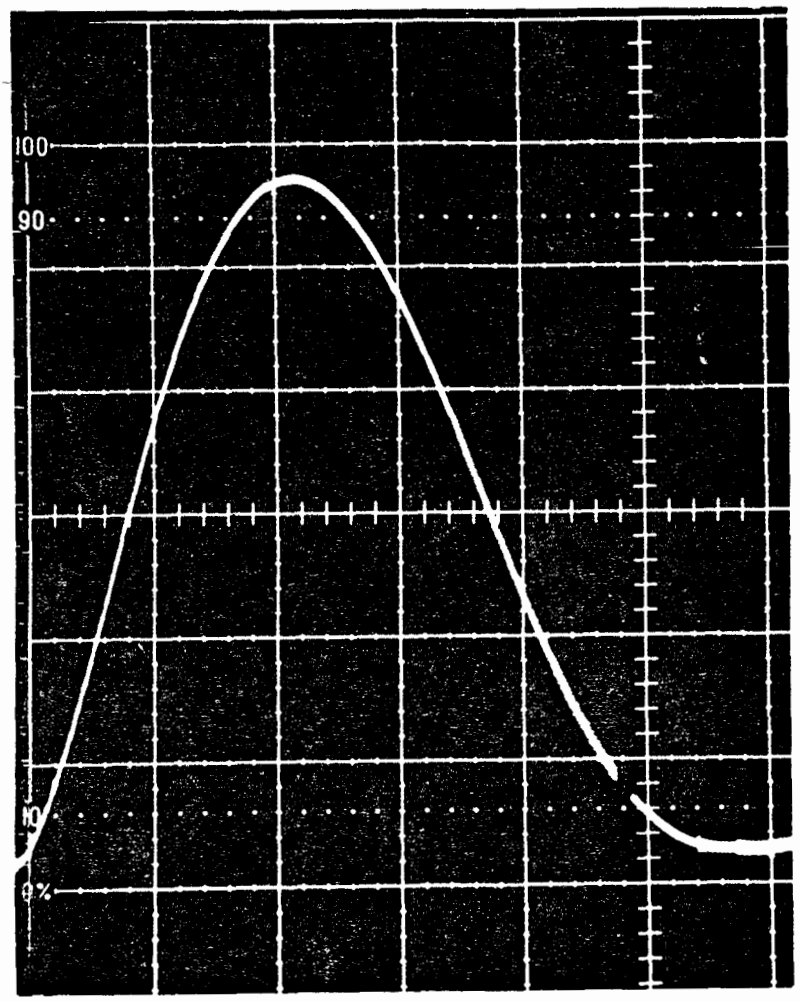

FIG III-4
INTENSITY OF PUMP PULSE AS A FUNCTION OF TIME; 500 μsec/div.

III-5 Laser Head and Cooling System

The laser head was designed for uniform flashlamp illumination of the laser rod. The highly polished aluminum inside surface forms a double-ellipse. The flash-tubes are positioned at the separate foci while the optic axis of the laser rod corresponds to the common focus. This geometry provides cylindrically symmetric pumping thus minimizing azimuthal variations of the population inversion.

The laser rod and flash-tubes were cooled with a flow of ∿½ liter/minute of distilled water. The arrangement is shown in Fig. III-4a. The water bath was temperature controlled with a Haake E52 thermostat and heater. The laser rod is cooled first so as to guarantee uniform cooling.

The water jackets were made of pyrex which absorbs the ultraviolet portion of the pump light. This is to avoid damage to the laser rod caused by solarization. The laser rod jacket was bonded to the lucite end-caps with a layer (∿1 mn thick) of G.E.-RTV silicone rubber as a necessary cushion against thermal expansion. All three coolant jackets were held in the laser head with nylon setscrews for stability and easy adjustment. Details of the laser head are shown in Figs. III-5 and III-6.

The laser head was mounted in a black plastic box supported on three spring-loaded screws on a 10" wide aluminum C-beam. This box reduced the intensity of extraneous pump

light. The inside of the box was covered with grounded copper sheet to shield the laboratory from the radiation noise of the trigger pulse.

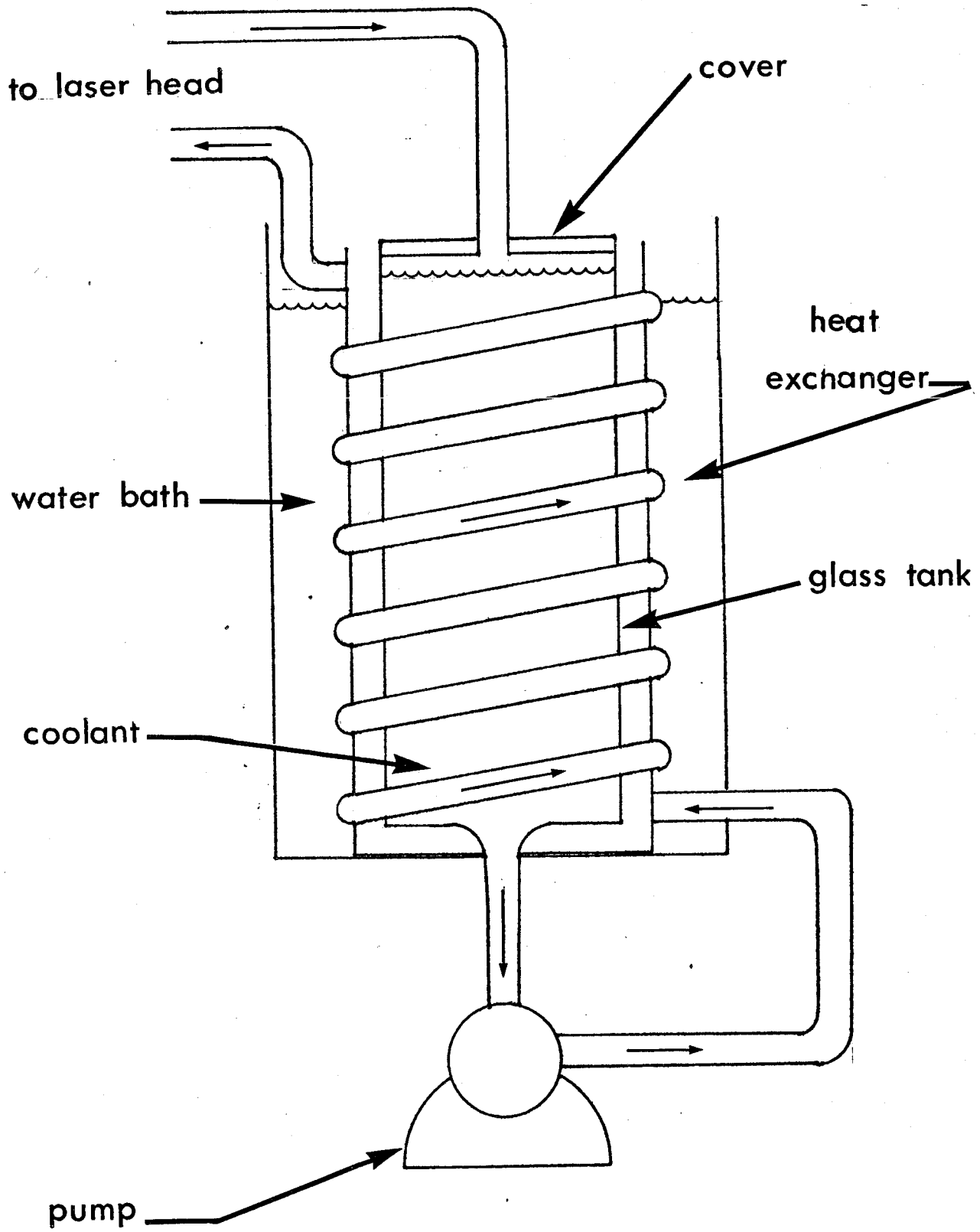

FIG. Ⅲ-4a Cooling System

TOP VIEW

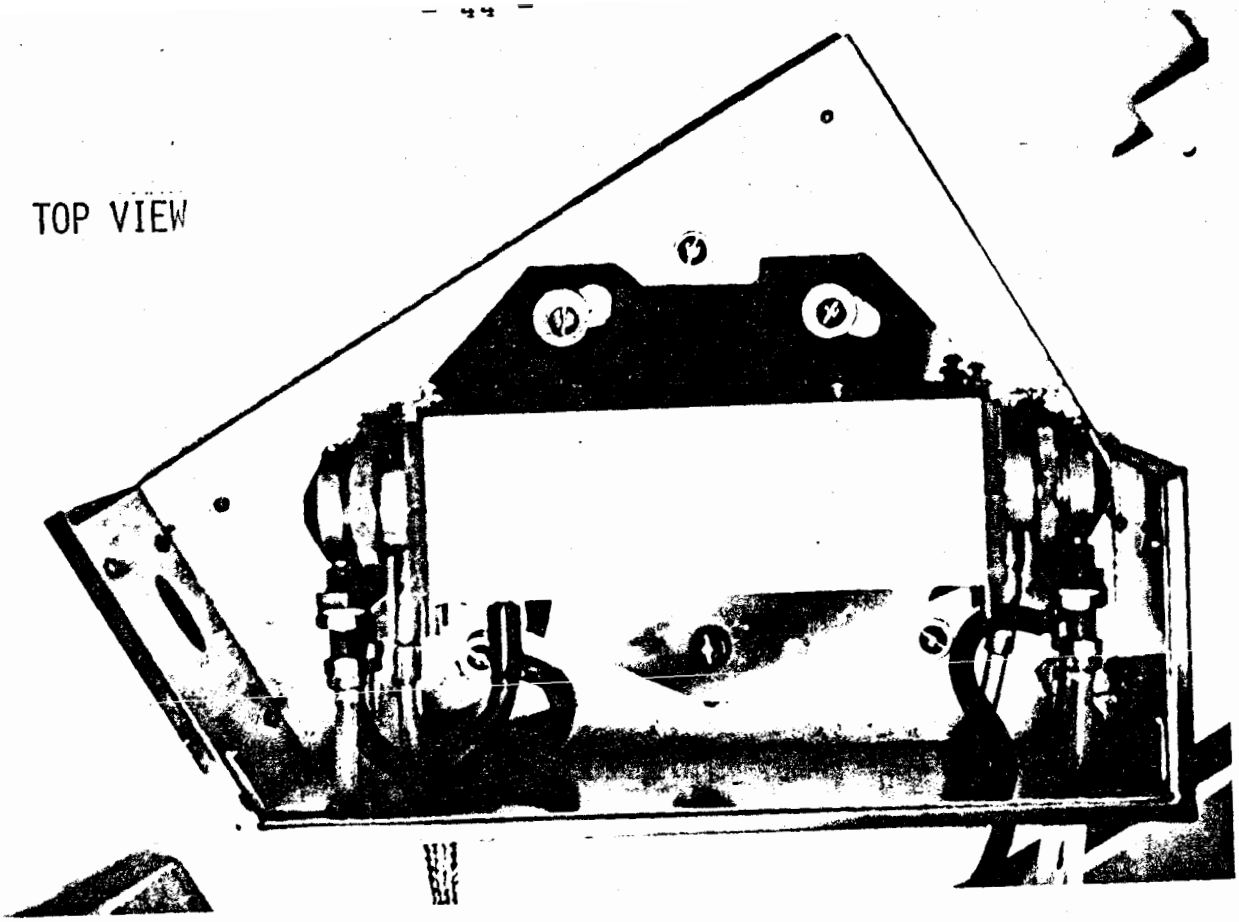

FRONT VIEW (OPEN)

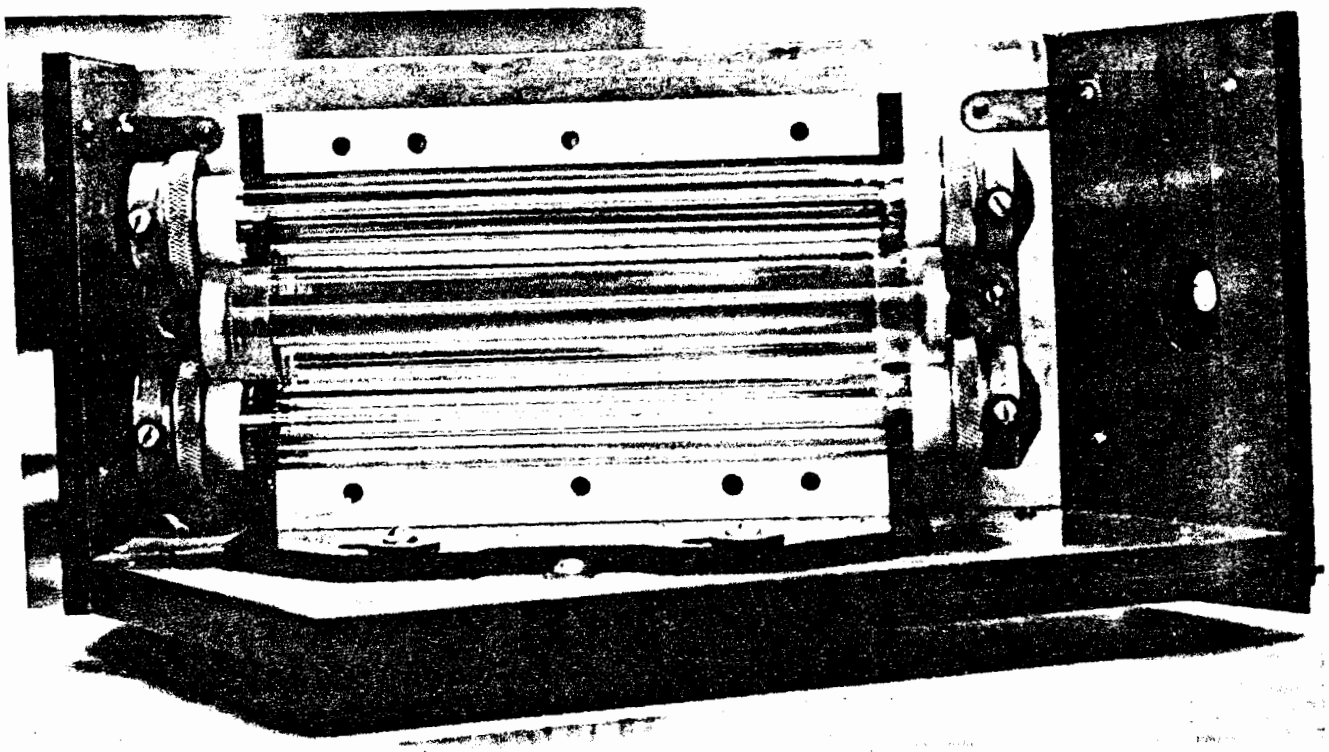

FIG III-5 LASER HEAD ASSEMBLY

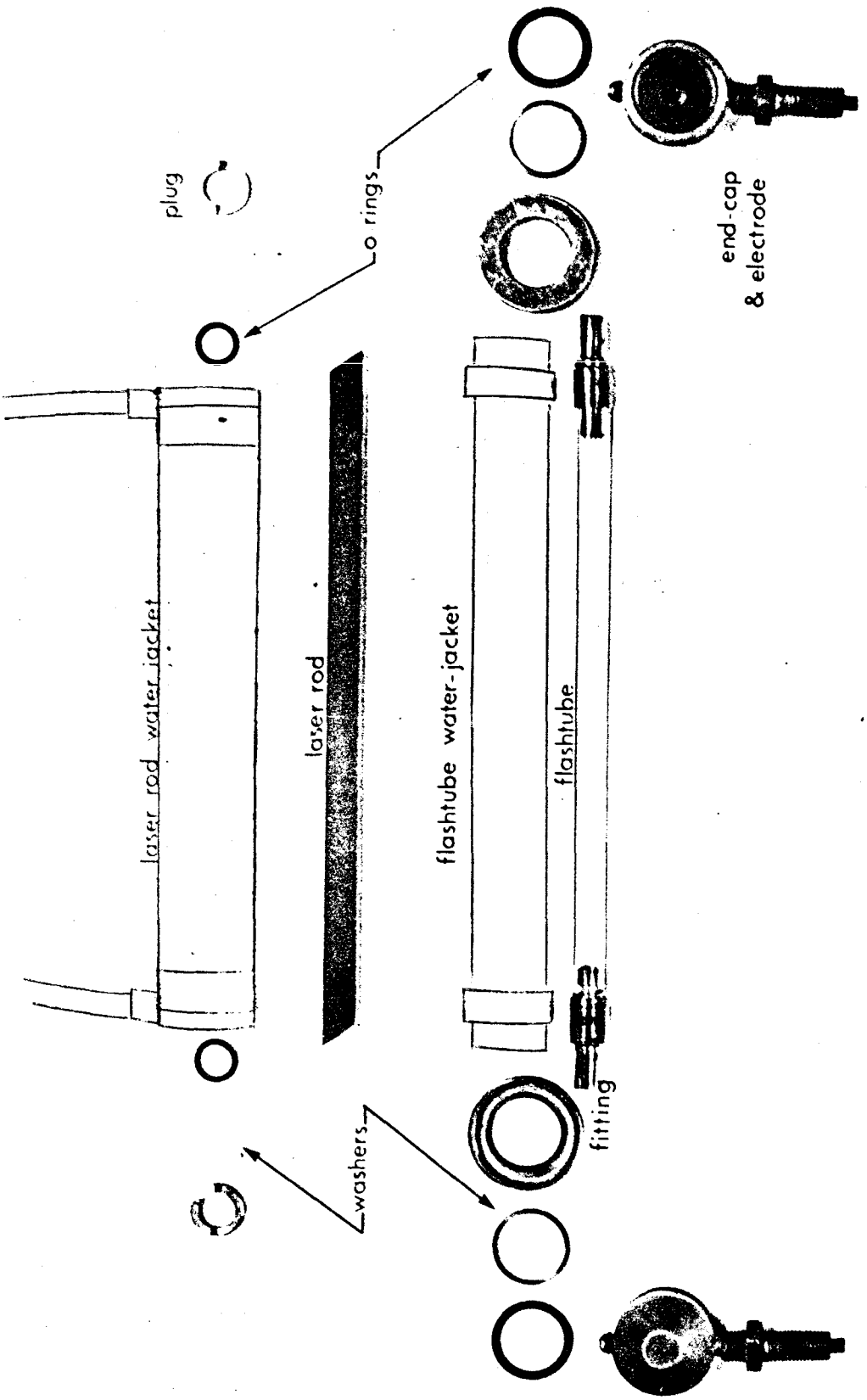

FIG III-6 CONSTRUCTION DETAILS

III-6 Q-Switch

The requirements of a passive Q-switch have been listed in Section II-3. The bleachable dye selected for this work was Kodak A9860. This dye with 1,2 dichloroethane used as the solvent has an absorption peak at 1.051 μ. It has an excited state life-time of 9.1×10^{-12} sec and is capable of withstanding the high power densities associated with Q-switched pulses. This dye breaks down quickly under blue and ultraviolet radiation so that pump light from the laser head should be minimized.

The optical cell for mode-locking was an Eastman 6088. This cell provides a 1.65 mm pathlength with a 35 mm aperture. The windows are made of a BSC-2 glass that is resistant to laser damage and accurately ground and polished. The external surfaces are coated for minimum reflection at 1.06 μ, thus eliminating the need for placing the cell at the Brewster angle.

CHAPTER IV

MEASUREMENTS OF PERFORMANCE AND DISCUSSION

IV-1 Free-Running Operation

Using the alignment procedure described in Section III-2, stimulated emission was attained with a threshold input energy of E_T = 500 joules. This condition was critically dependent on the alignment which required adjustment to within 5×10^{-4} radians.

The emission spectrum was obtained with a 3/4 - meter Czerny-Turner spectrometer. A fraction ($\sim$10%) of the output obtained from a glass beam splitter was aligned incident on an opal glass plate providing a diffuse source of emission radiation. The entrance slit of the spectrometer was placed 50 cm from this source and the single pulse spectrum was photographed using Kodak 1-Z infrared-sensitive plates.

Fig. IV-1 shows the relative intensity profile obtained from photodensitometer traces for several input energies. With higher pumping energy more of the laser transition line-width comes under the stimulated emission gain curve resulting in the observed broadening of the emission spectrum.

The output energy of the laser was measured with a Hadron Model - 108 ballistic thermopile. The laser pulse is absorbed in a metal cone and the resulting temperature difference between this and another identical reference cone results in a thermocouple potential which is proportional to the total energy absorbed. The instrument has a sensitivity of

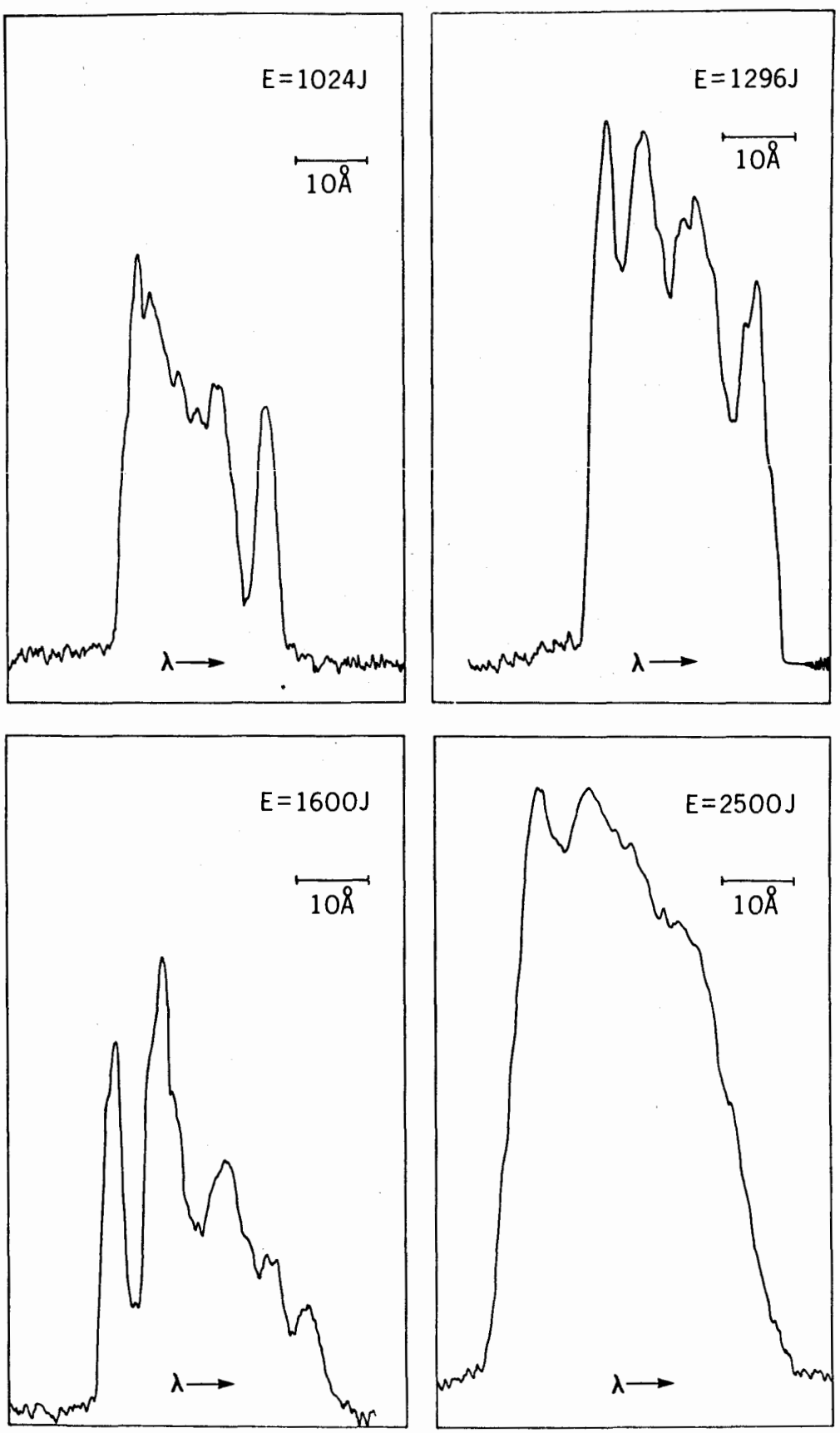

FIG IV-1

EMMISSION SPECTRA FOR FREE RUNNING SINGLE PULSES AT DIFFERENT ENERGIES. DIFFERENT VERTICLE SCALES FOR EACH PROFILE.

54.1 μ volts/joule. Fig. IV-2 shows the output energy, E_{out}, as a function of pump energy, E_{in}.

The time evolution of the emission was observed with a Tektronix 555 oscilloscope and an RCA 925 photo diode detector. Fig. IV-3 shows the normal spiked emission characteristic of a solid state laser. This behavior is usually explained in terms of a competition between the filling and depletion rates of the upper laser level. Whenever this level is emptied faster by stimulated emission than it is being filled by the pumping process, the inversion can fall below threshold and lasing will cease until population inversion is achieved again. The result is a sporadic fluctuation of the output intensity.

The far-field beam divergence was obtained from the variation of the beam spot size with distance from the resonator. The spot size was estimated from the diameter of the well-defined pattern burned in a developed, but unexposed Polaroid 3000 film. This method assumes a square profile for the radial variation of intensity across the beam. With an input energy of 800 joules typical values for the beam divergence were $1\text{-}3 \times 10^{-4}$ radians.

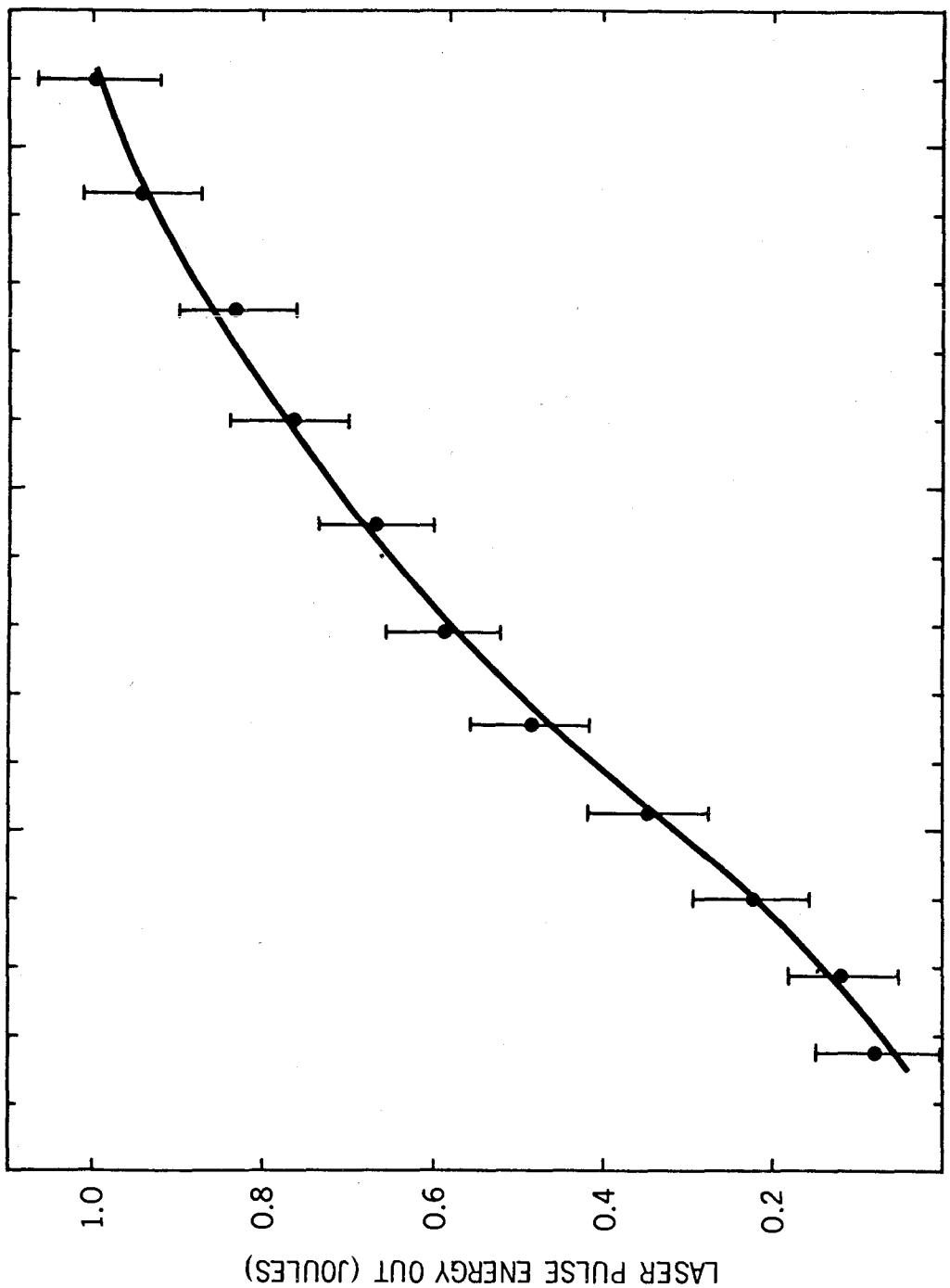

FIG IV-2

LASER OUTPUT ENERGY, E_{out} AS A FUNCTION OF THE ELECTRICAL INPUT ENERGY E_{in}

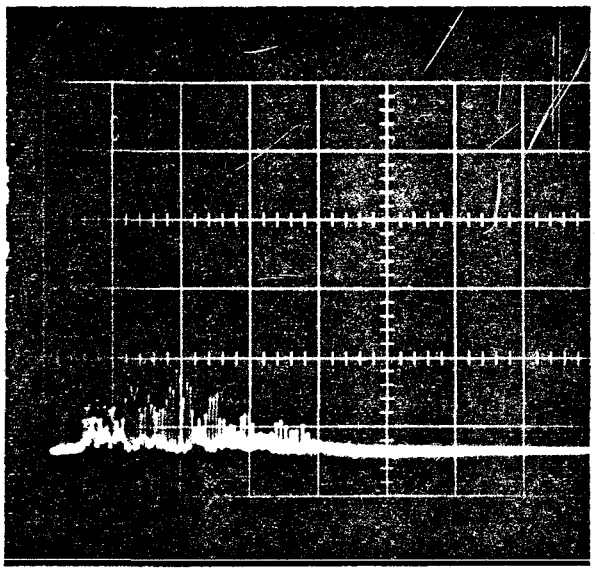

680 JOULES

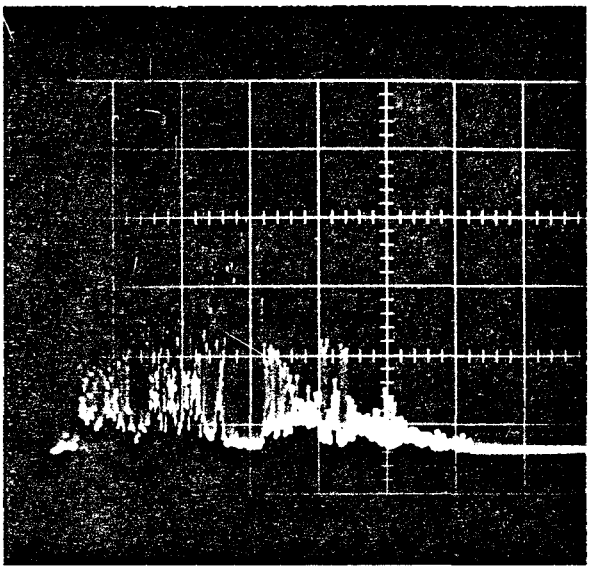

1010 JOULES

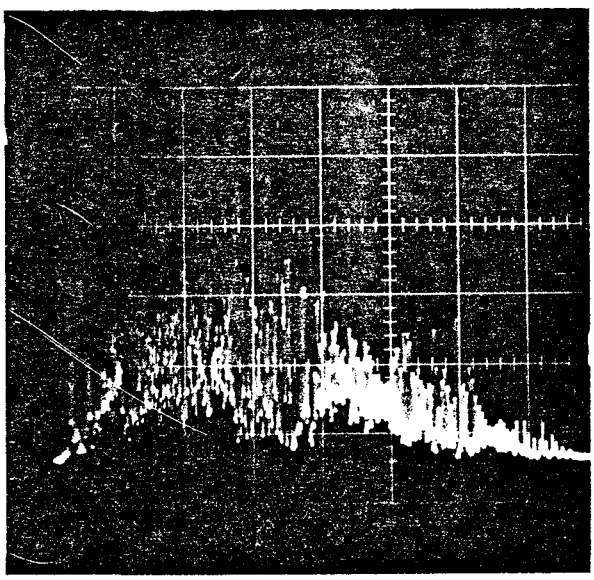

1400 JOULES

FIG IV-3 TIME EVOLUTION OF FREE EMISSION
TIME SCALE IS 200μ SEC/DIV

IV-2 Thermal Lensing

In the course of the above measurements it was observed that the threshold energy was higher than usual after the laser had been allowed to "rest" for some time. Subsequent shots exhibited lower thresholds and higher output energies. Several experiments were carried out in an effort to explain this phenomena and to describe its associated effects.

The output energy was measured with the ballistic thermopile as a function of the delay time, τ, between successive shots. The result is shown in Fig. IV-4. The effect of the delay time is noticeable for τ 30 seconds and results in a four-fold enhancement of energy efficiency at τ = 5 seconds.

The phenomena was shown to be associated with thermal effects by introducing a sudden change in the coolant temperature and observing the output energy. The laser was allowed to rest for several minutes. The circulation system was then turned off and the heat bath temperature was reduced by 15^{o}C with ice. The circulation was resumed and the laser fired a few seconds after the rod experienced the sudden drop in temperature. The output energy was considerably increased just as with short delay times between successive shots.

Optical distortion of the laser rod was then observed during the pumping-cooling cycle as well as during the sudden cooling with the ice-water. With the mirrors removed a He-Ne probe beam was passed through the laser rod and its cross-section observed on a white screen several meters away. The

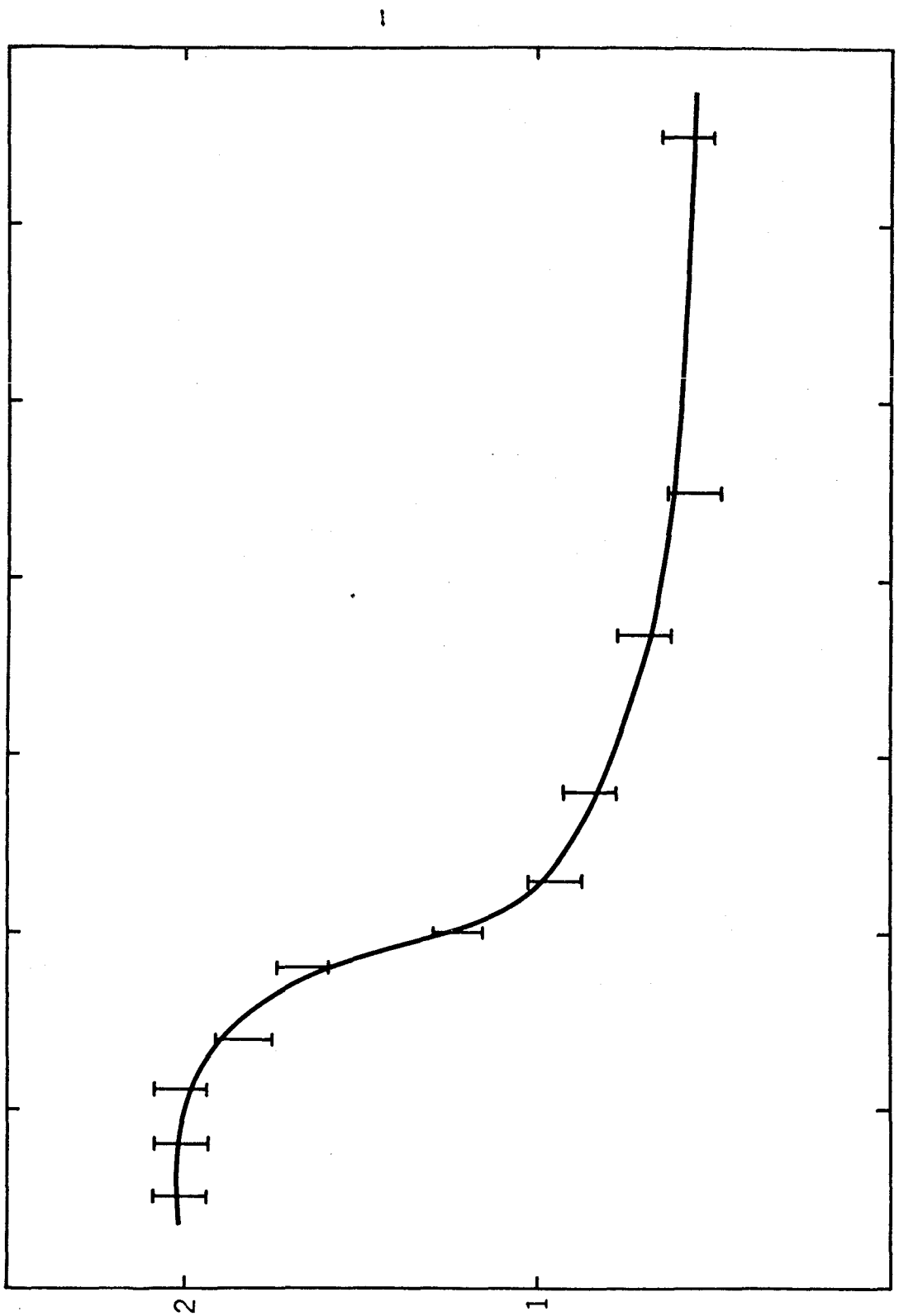

FIG IV-4

LASER OUTPUT ENERGY E_{out}, MEASURED AS A FUNCTION OF THE DELAY TIME BETWEEN PULSES τ

beam had been telescoped to a width identical with the rod diameter and giving minimum divergence.

When the ice-water began cooling the rod, a cycle of focussing and over-focussing was started. Typical behavior of the probe beam spot shape is sketched in Fig. IV-5. The whole cycle was essentially completed within about 30 seconds.

The focussing cycle can be explained in terms of two focal lengths or cylindrical aberration. The focussing is stronger in the horizontal plane (containing the Brewster angle) than the vertical. At a stage B, the focussing is predominately horizontal, while at stage C with maximum focussing both the vertical focussing and horizontal over-focussing are apparent. The process then reverses itself, relaxing to its initial state after 30 seconds.

The results obtained for ordinary pumping and cooling were similar with one notable exception. A diverging lens effect lasting less than 1 sec appeared immediately with each pump flash.

The focal lengths in the two orthagonal planes were measured with a Polaroid camera back and Polaroid 3000 speed film using neutral density filters to attenuate the probe beam. The film was exposed at various distances from the rod at the same time in the focussing cycle. The variation of spot size with distance afforded a rough measure of the focal length. Typical minimum values were 5 meters in the vertical plane and 2 meters in the horizontal plane.

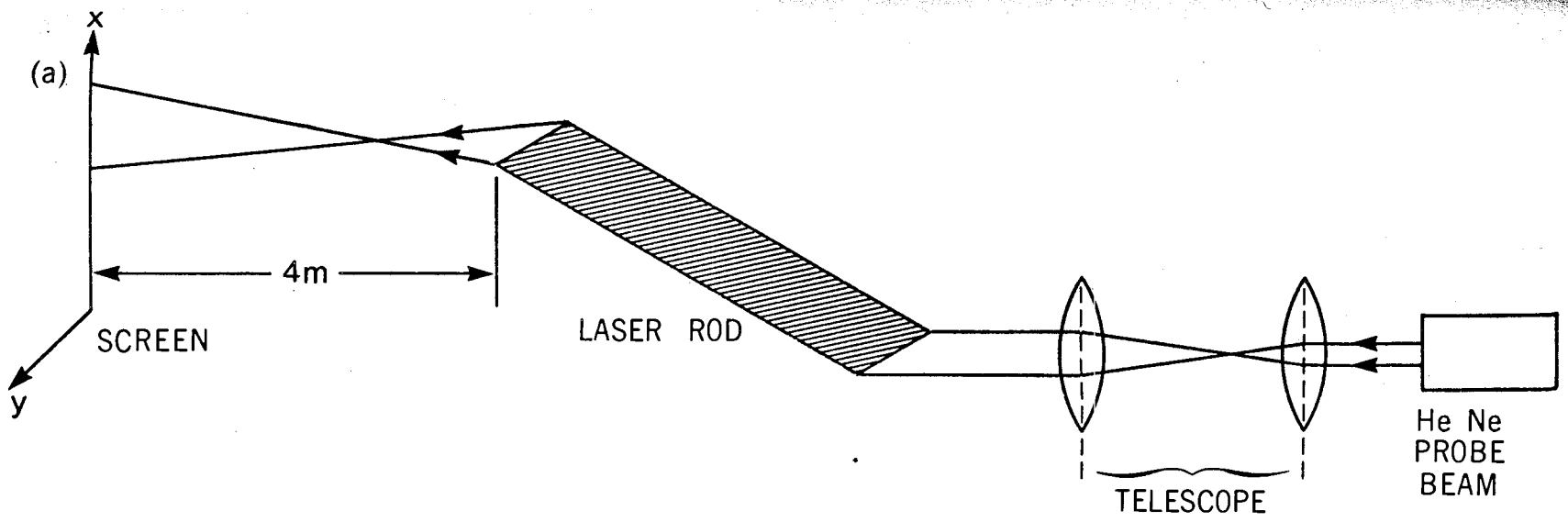

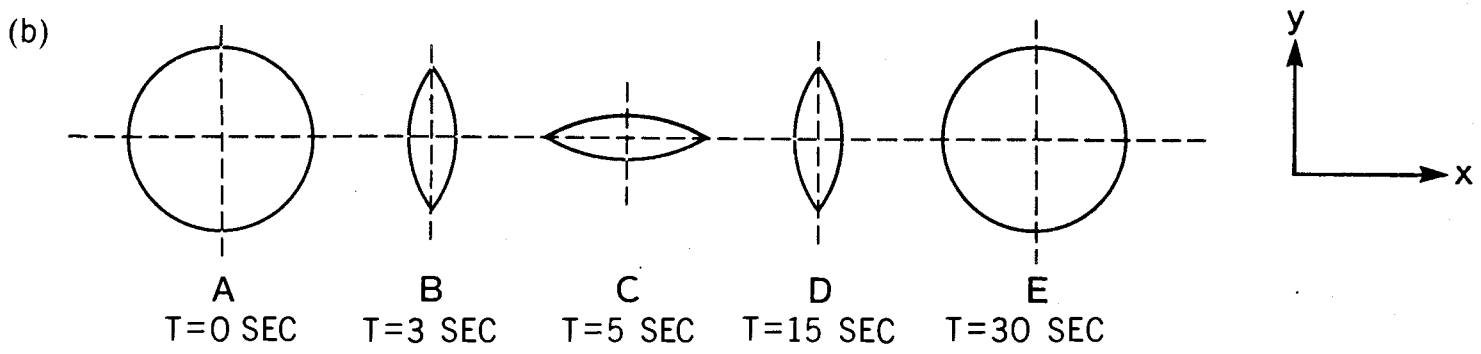

FIG IV-5

a) EXPERIMENTAL SET-UP FOR OBSERVING THERMAL LENSING

b) SKETCH OF TIME EVOLUTION OF THE PROBE BEAM CROSS-SECTION AT SCREEN. T IS THE TIME FROM THE ONSET OF COOLING

Other characteristics were also seen to depend on the cooling process. The far-field beam divergence increased with repetition rate (smaller τ), the divergence in the horizontal plane being larger than in the vertical plane. Also, the emission characteristics progressed from the usual relaxation spiking to quasi-continuous emission (see Fig. IV-6) with higher firing rate.

Similar measurements were also made using the Schott LG56 glass rod with the same ion doping (3%). This glass is designed to minimize thermal effects by compensating for the positive contribution to the temperature dependence of optical path length due to linear expansion, with a negative temperature coefficient of refractive index. The manufacturers claim a value of $K = 2.3 \times 10^{-6}$ $(°C^{-1})$ for the temperature dependence of the optical path length. The lensing effects were qualitatively the same though noticably less severe.

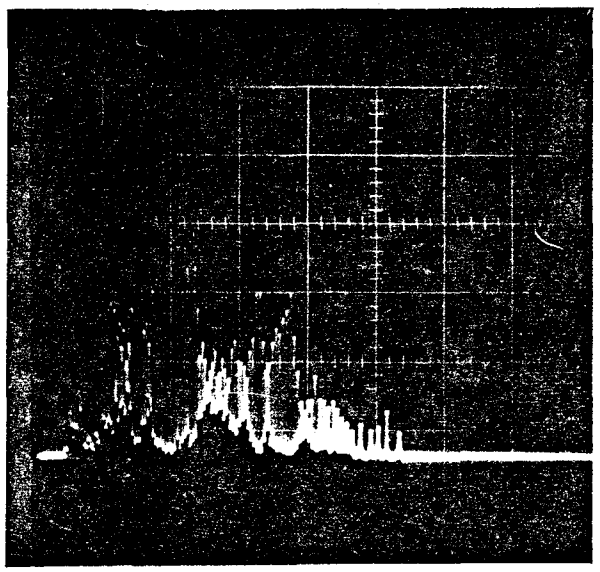

T=60 SEC
0.02 V/DIV

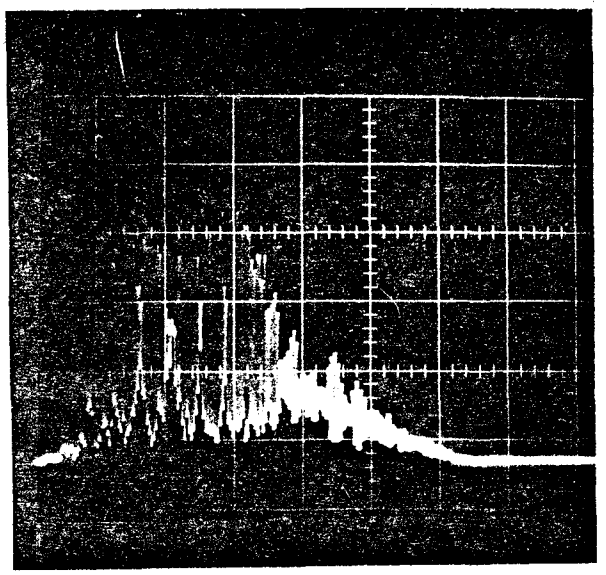

T= 30 SEC
0.02 V/Div

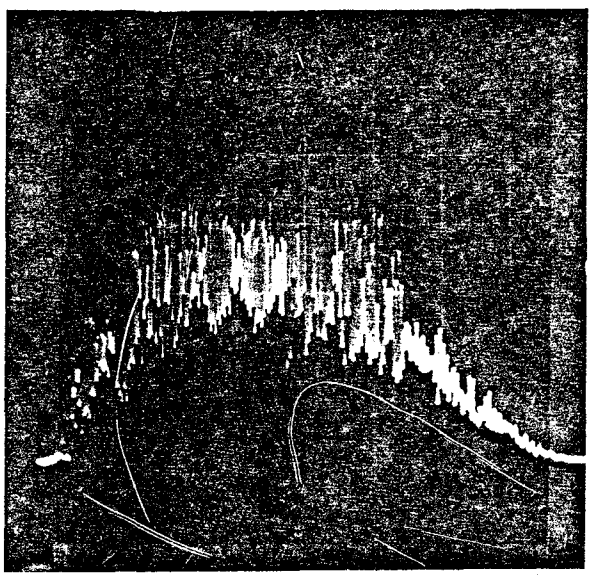

T=15 SEC
0.02 V/DIV

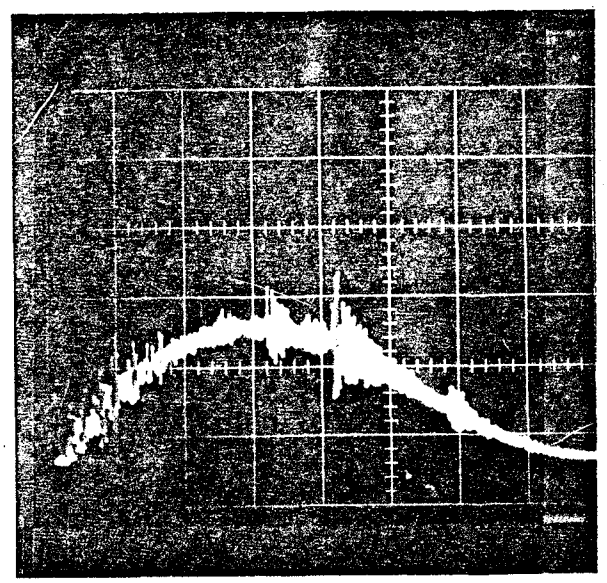

T=5 SEC
0.05 V/DIV

FIG IV-6 TRANSITION FROM RELAXATION SPIKES TO QUASI-CONTINUOUS EMISSION WITH SHORTER DELAY BETWEEN LASER SHOTS
TIME SCALE IS 200μ SEC/DIV

IV-3 Discussion of Thermal Lensing

The behavior described above can be explained in terms of a theory of thermal lensing in which pump induced radial thermal gradients produce a lens-like medium in a laser rod. Some effects of thermal lensing have been observed with lasers operating at high pulse rates or in cw mode (O.N. Voronkin et al. 1966; Osterink and Foster 1968; Koechner 1970).

Thermal gradients can arise in two ways. Non-uniform heating by the pump radiation, the surface becoming hotter than the center, results in a weakly diverging lens effect during the pump pulse itself (Burnham 1970; Chun and Bischoff 1971). The heated rod, subsequently being cooled at its surface, assumes a reversed temperature gradient (hotter at the center), and consequently becomes a strong positive lens, the focal length being a function of time as the rod cools.

The optical path length $s = n_0 \ell$ through a distance, ℓ, in material having an index of refraction, n_0, in general depends on the temperature, T, as

$$\frac{dS}{dT} = \frac{d(n_0 \ell)}{dT} = \ell \frac{dn_0}{dT} + n_0 \frac{d\ell}{dT} \qquad (1)$$

Then the fractional change in the optical path length between two planes (resonator mirrors) is

$$K \equiv \frac{1}{\ell}\frac{dS}{dT} = \frac{dn_0}{dT} + (n_0 - 1)\alpha \qquad (2)$$

where $\alpha = \frac{1}{\ell}\frac{d\ell}{dT}$ is the coefficient of thermal expansion and $\frac{dn}{dT}$ is the intrinsic temperature coefficient of the index of refraction. This can be rewritten in terms of a generalized index of refraction $n = \frac{s}{\ell}$ as $K = \frac{dn}{dT} = \frac{dn_0}{dT} + (n_0 - 1)\alpha$. A typical laser glass has $K = 0.43 \times 10^{-5}\ C^{0-1}$ (A.O. # 3835).

Now, a laser rod being cooled through its surface which is maintained at a constant temperature will assume a radially quadratic temperature distribution (Koechner 1970). With the above linear dependence of the refractive index on the temperature we can write in terms of the radius, r,

$$n(r) = n_0\left(1 - \frac{r^2}{b^2}\right) \qquad (3)$$

Here b is a measure of the strength of the index variation.

Kogelnik (1965) has calculated the ray transfer matrix (RTM) for a length, ℓ, of such a lens-like medium having an average index of refraction, n, and with its end surfaces normal to the optic axis. The RTM relates the position, x, and slope, x′, of a ray in the output plane to the corresponding input parameters (x_0, x_0')

$$\begin{pmatrix} x \\ x' \end{pmatrix} = \begin{pmatrix} \cos\frac{2\ell}{b} & \frac{b}{2n}\sin\frac{2\ell}{b} \\ \frac{-2n}{b}\sin\frac{2\ell}{b} & \cos\frac{2\ell}{b} \end{pmatrix} \begin{pmatrix} x_o \\ x_o' \end{pmatrix} \qquad (4)$$

By applying Snell's law to the refraction of an elementary pencil incident at Brewster's angle, α, and considering the accompanying change in beam width, we find the corresponding RTM for Brewster-Brewster configuration to be (see Appendix B)

$$\begin{pmatrix} x \\ x' \end{pmatrix} = \begin{pmatrix} \text{Cos}\,\frac{2\ell}{b} & \frac{b}{2n^3}\,\text{Sin}\,\frac{2\ell}{b} \\ \frac{-2n^3}{b}\,\text{Sin}\,\frac{2\ell}{b} & \text{Cos}\,\frac{2\ell}{b} \end{pmatrix} \begin{pmatrix} x_o \\ x_o' \end{pmatrix} \qquad (5)$$

Note this expression holds only for the case $\tan \alpha = n$.

An optical system described by a RTM

$$\begin{pmatrix} A & B \\ C & D \end{pmatrix}$$

has a focal length $f = -\frac{1}{C}$. Equation (4) gives the tangential focal length $f_T = \frac{b}{2n \sin 2\ell/b}$, and equation (5) yields the sagittal focal length $f_s = \frac{b}{2n^3 \sin 2\ell/b}$. We thus find the ratio of these foci to be $f_T/f_s = n^2$.

This last result describing the astigmatism associated with the Brewster-Brewster rod geometry agrees with the observed ratio of focal lengths. The Owens-Illinois rod has $n^2 = 2.3$ and we measured $\frac{f_T}{f_s} = 2.5$. This is more than reasonable considering the experimental accuracy in a dynamic situation (±25%).

The effects associated with output energy and emission features can qualitatively be ascribed to thermal lensing in

terms of equivalent resonator theory. Kogelnick (1965) has shown a Fabry-Perot resonator with an internal focussing element of focal length f to be equivalent to an empty spherical cavity with mirror curvature R = 2f. Now the usual resonator theory characterizes the spherical resonator with a higher Q and larger beam divergence than is found with the plane-parallel resonator. And here it appears that the residual positive focussing (from previous shots) compensates for the short-lived diverging lens effect due to the initial non-uniform heating. Thus we can expect a large increase in the energy output in going from a cavity with slightly negative mirror curvature to a strongly positive curvature.

The spherical cavity also allows more off-axis modes to oscillate simultaneously. This appearance of many spatial mode limits the usual single mode saturation-relaxation process responsible for normal spiked emission.

The pulse rate thus strongly influences the laser output characteristics by determining the degree of residual lensing under which the laser is operated. The Schott glass with its reduced thermal effects is the preferred host material for single mode, low divergence output.

Considering all the effects associated with thermal lensing a pulse rate of 4 pulses per minute was considered to be optimal. Unless otherwise stated, this pulse rate may be assumed in the following discussions.

IV-4 Mode-Locked Operation

The laser was successfully Q-switched with the absorber low-level transmission ranging between 60% and 95%. With a free-running threshold energy E_F = 500 joules at a pulse rate of 4 ppm the Q-switched threshold began at $E_Q = 1.4\ E_F$ for a Q-switch low level transmission of T = 95% and increased to $E_Q = 4\ E_F$ with T = 60%.

The Q-switched energy output was an order of magnitude smaller than for the corresponding free-running operation. A typical pulse had an energy of 200 millijoules and a duration of 100 nsec. This corresponds to an average power of 2 megawatts.

Observation of the time evolution of these Q-switched pulses revealed the pulse train substructure characteristic of mode-locked operation. The pulses were detected with an Optics Technology Inc. Model 620 ultra-fast-detector having a rise-time τ_1 = 0.3 nsec and displayed on a Tektronix 519 travelling wave oscilloscope having a rise-time τ_2 = 0.35 nsec. The rise-time of this combination is thus

$$\tau = (\tau_1^2 + \tau_2^2)^{\frac{1}{2}} \cong 0.5 \text{ nsec}.$$

Fig. IV-7 shows a typical oscilloscope trace of a Q-switched pulse as recorded on Polaroid 10,000 speed film. The Q-switched envelope is seen to consist of ∿20 equally spaced pulses of length 1.5 nsec and separated 7.5 nsec.

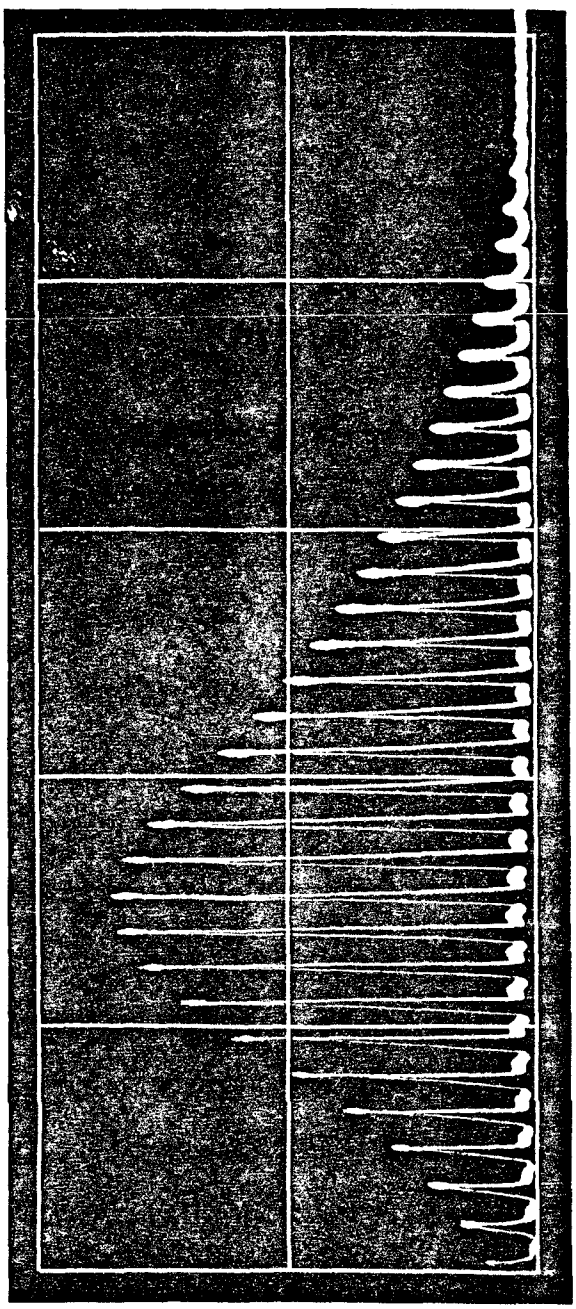

FIG IV-7 OSCILLOSCOPE DISPLAY OF A TYPICAL MODE-LOCKED PULSE TRAIN. TIME SCALE IS 50 NSEC/DIV.

These results were obtained with a cavity optical path length of 1.12 meters including the correction due to the dye cell. As shown in Section II-2 the period of a mode-locked pulse train is given by

$$T = \frac{2 L_{opt}}{C} = 7.5 \times 10^{-9} \text{ sec.}$$

which is in complete agreement with observation.

The observed width of 1.5 nsec for the individual pulses represents only an upper limit for the actual pulse duration since this time interval is the minimum resolvable considering the 0.5 nsec overall rise-time.

These oscilloscope traces provided other information concerning the mode-locked operation. Although the output energy remained essentially constant for given experimental conditions, the width of the pulse train envelope varied considerably with the number of pulses ranging between 10 and 40.

The pulse trains were not always "clean" but often consisted of multiple trains having random relative phase. These multiple trains occurred more often when the dye cell was not adjacent to a cavity mirror and when the input energy was well above threshold. However, with introduction of internal thermal lensing as occurs with a pulse rate of 4 ppm, these multiple pulse trains were almost completely eliminated. This alone justifies the use of higher repetition rates.

The emission spectrum of the mode-locked laser was photographed as outlined in Section IV-1. In this case the emission was characterized by a uniform spectrum approximately 50Å wide without the many individual lines present in the free-running emission spectra (c.f. Fig. IV-1). The loss of structure indicates the tendency of the saturable absorber to distribute the energy uniformly throughout the spectral line-width of the laser medium by the generation of side-bands at the Fabry-Perot resonances of the optical cavity.

IV-5 Pulse Length Measurements

As mentioned above, the photo-diode and oscilloscope combination provides only an upper limit on the pulse length. Section II-4 outlined the theory of an intensity correlation method which provides a direct measurement of very short pulse lengths.

The experimental method (see Fig. IV-8) consists essentially in reflecting the output beam back onto itself from a mirror immersed in a dye exhibiting two-photon absorption at the laser wavelength, 1.06 μ. The resulting fluorescence was photographed from the side thus obtaining the spatial variation of the auto-correlated intensity. In particular, the variation adjacent to the mirror should correspond to each pulse folding onto itself giving a measure of the pulse half-length.

It was found that with this mirror properly aligned normal to the beam the resulting feedback onto the laser cavity destroyed the pulse-train structure leaving only the Q-switched envelope. The necessary isolation was achieved by removing the measurement apparatus to a position ∿5 meters from the laser cavity so that a slight misalignment of the T.P.F. mirror would eliminate feedback into the cavity.

The glass dye-cell was 10 cm on a side and 2 cm wide. The mirror was dielectrically coated for 100% transmission at 1.06 μ. It was cut in half along its diameter allowing the absorption to take place near one wall of the dye cell. This technique minimized self absorption of the fluorescent radiation. The

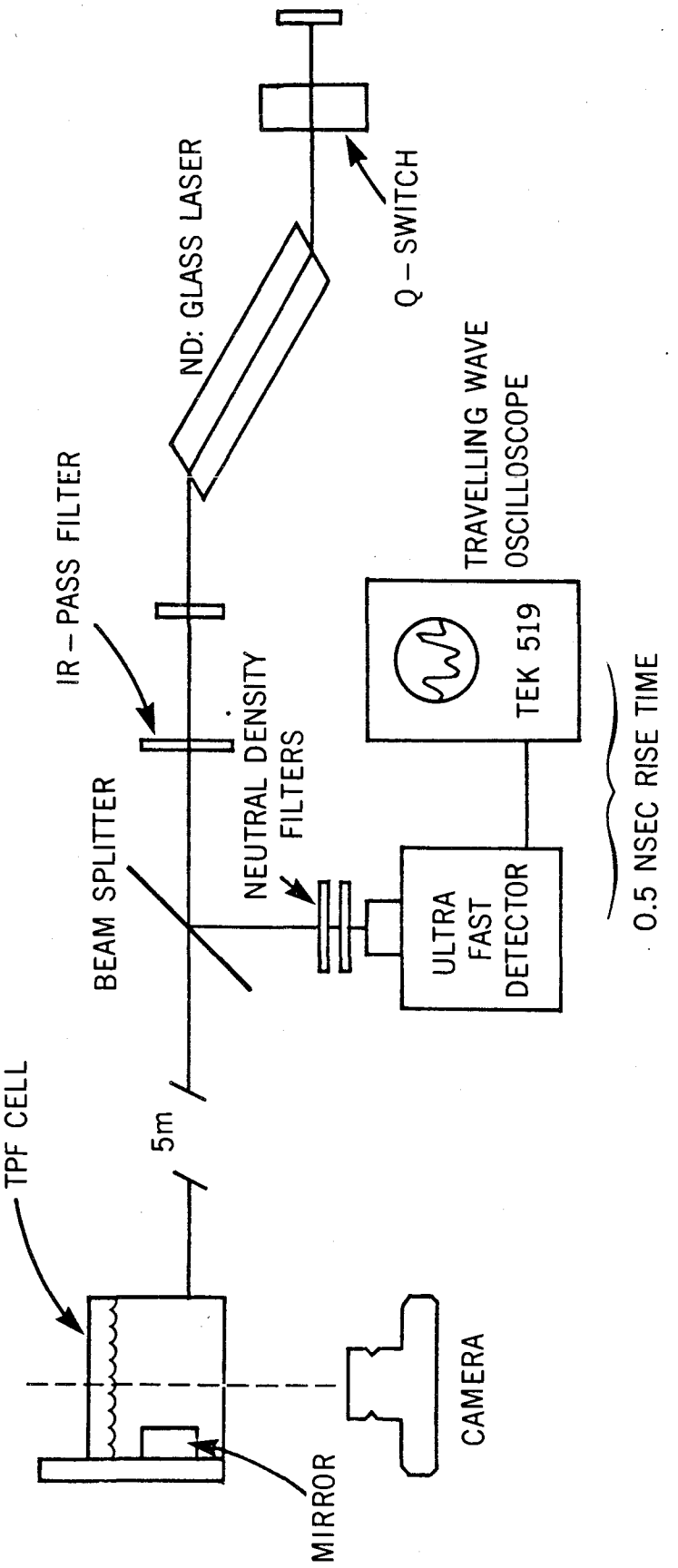

FIG IV-8
EXPERIMENTAL SET-UP TPF PULSE LENGTH MEASUREMENT.
THE IR-PASS FILTER REMOVES THE VISIBLE PORTION OF THE PUMP LIGHT

mirror was expoxied to a plastic strip which could be attached at various heights to one end of the cell.

The dye chosen for this measurement was Rhodamine G. In an ethanol solution this dye has its primary absorption peak at 5300Å (see Fig. IV-9) which is close to the second harmonic of the Nd:glass laser. The conversion efficiency is high; the fluorescence from the mode-locked laser was easily visible.

The fluorescence was identified using a ½ meter Jarrel-Ash spectrometer. The output from a photomultiplier tube as displayed on a Tektronix 555 oscilloscope peaked at 5820A. No fluorescence was observed at shorter wavelengths from possible upper excited states.

With the camera and dye cell properly shielded from extraneous pump light the fluorescence was photographed with an 86 mm f:1.2 lens using Polaroid 10,000 speed film. To obtain photodensitometer traces, the Polaroid positive was photographed with a Cannon Macro-lens to produce a 35 mm negative. A typical photograph, along with its photo-densitometer trace, is shown in Fig. IV-10.

The half-width of the pulse convolution is about $\Delta\ell$ = 1 mm. Assuming the index of refraction of the liquid to be n = 1.5, this corresponds to a pulse length of

$$\tau = \frac{n\,\Delta\ell}{c} = 5\times10^{-12}\ \text{sec}\ .$$

(Under typical operating conditions of 20 pulses with a total

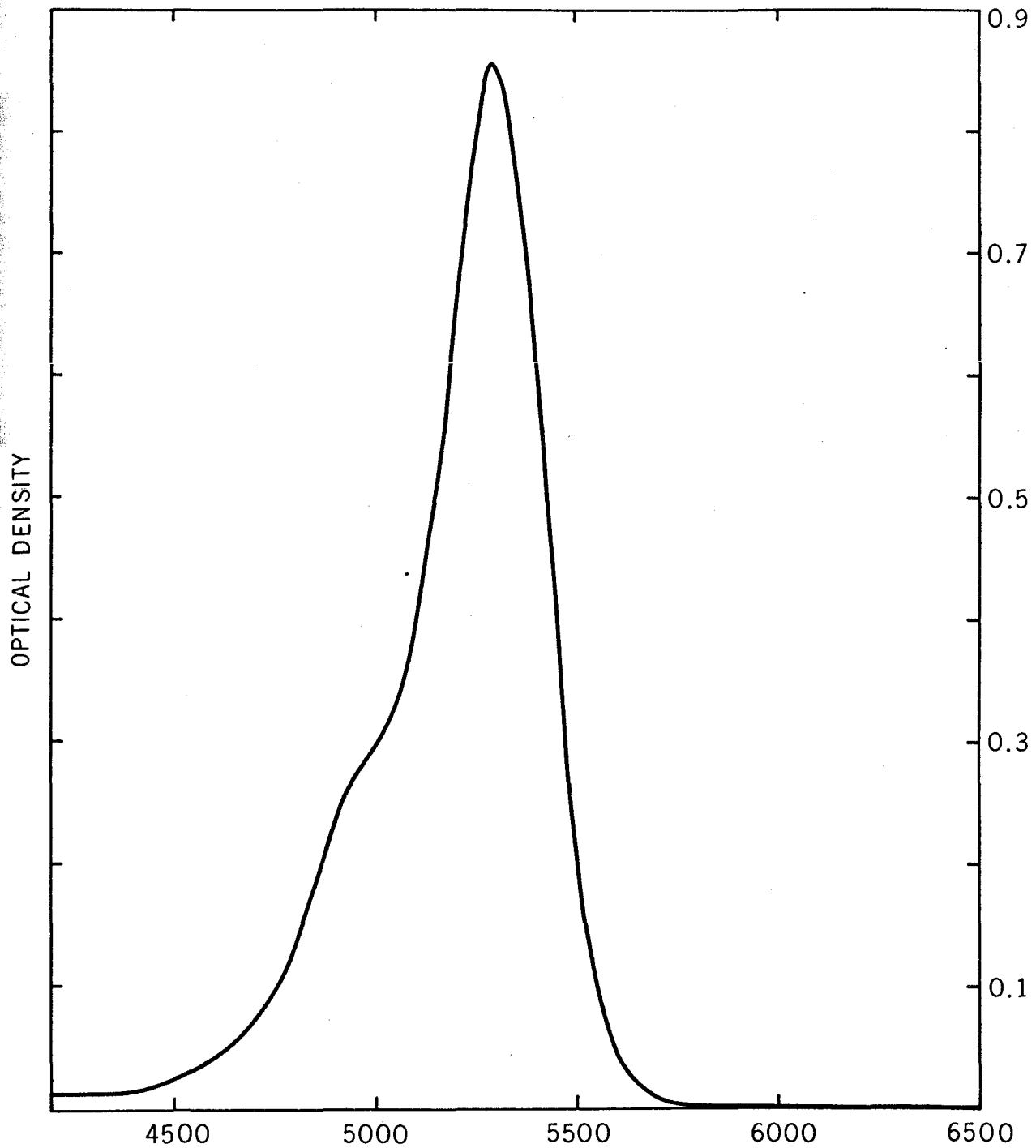

FIG IV IV·9

ABSORPTION SPECTRUM OF RHODAMINE G IN METHANOL (5mg/ml)
AGAINST METHANOL. PATH LENGTH 0.1mm

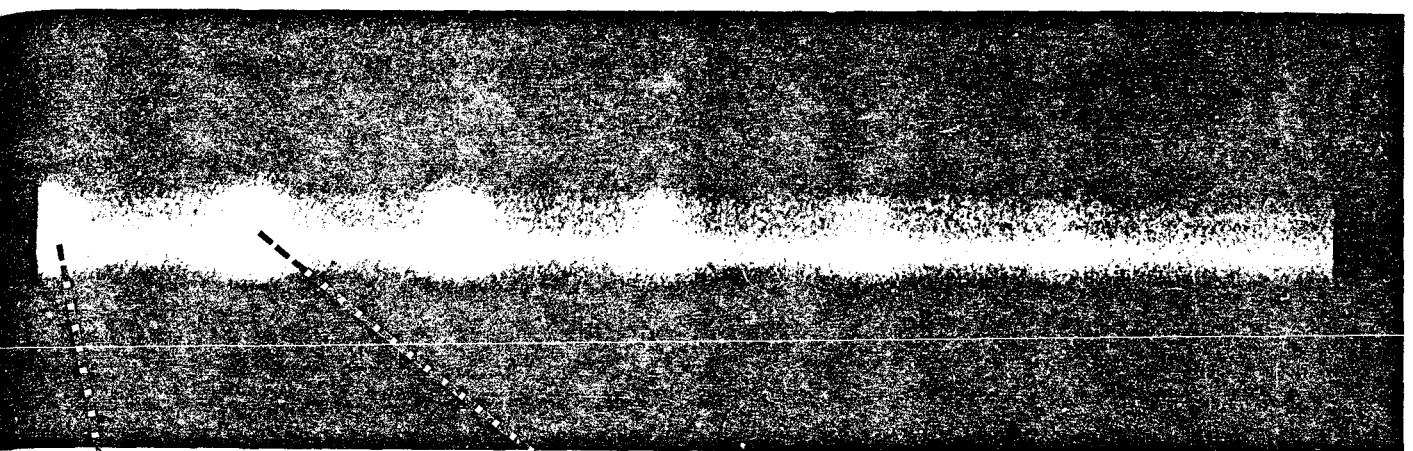

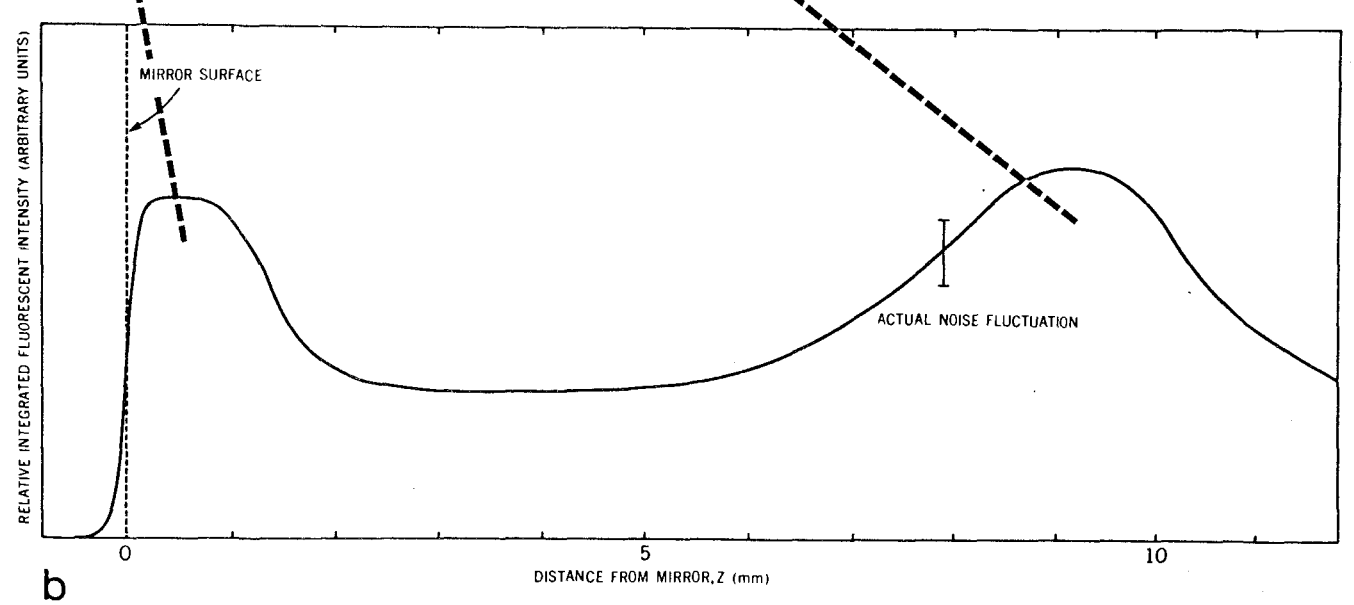

b

FIG. IV-10

a) PHOTOGRAPH OF TPF TRACE SCALE 1:1

b) RELATIVE FLUORESCENCE TAKEN FROM PHOTODENSITOMETER PROFILE (ACTUAL TRACE HAS S/N RATIO ≈ 10)

energy of 200 millijoules this pulse length corresponds to unfocussed peak powers of ∿2 gigawatts!)

As pointed out in Section II-4, this is the value of a band-width limited short pulse only if the contrast ratio of the fluorescent intensity is R = 3 rather than R = 1.5 as would be the case for randomly phased modes. The densitometer gives a value of R = 2.7 ± 0.2, indicating a strong degree of mode-locking.

With a mode-locked emission bandwidth of 50Å, the theoretical lower limit for pulse length is 6×10^{-13} sec. Our measurement being larger by an order of magnitude is a general result in mode-locking experiments. Treacy (1968) has shown that a frequency dependent index of refraction within the cavity causes frequency modulation or chirping of the mode-locked pulses.

If we expand the index of refraction in a Taylor series about the carrier frequency, ω_0

$$n = n_0 + \frac{dn_0}{d\omega}(\omega-\omega_0) + \frac{d^2n_0}{d\omega^2}(\omega-\omega_0)^2 + \cdots$$

and substitute into the expression for the closed loop phase shift $\phi = \frac{2\pi Ln}{c}$ we can write

$$\phi = \alpha + \beta(\omega-\omega_0) + \gamma(\omega-\omega_0)^2$$

Culter (1955) has shown that the quadratic term results in the

instantaneous frequency being swept linearly through the pulse at a rate determined by γ. It is as though the higher frequencies have a longer cavity circulation time and hence lag behind the low frequency components.

Treacy was able to compress such pulses by a factor of 2 by arranging a pair of plane blazed gratings so as to provide an optical path proportional to the wavelength. It is not known whether the dye or laser medium is responsible for the chirp characteristics of Nd:glass pulses.

The appearance of pulse groups separated by $\sim$1 cm or 50 psec as shown in Fig. IV-10 can be explained (DeMaria 1969) in terms of multiple cavities. If a partially reflecting surface, S, is introduced into the resonator, new cavity lengths will be created corresponding to multiple reflections between S and the nearby cavity mirror. Additional pulses will be generated, separated by the round trip time between S and the mirror. In these experiments it was found that the pulse separation increased proportionately with the distance between the Q-cell and cavity mirror.

There is another explanation of this sub-structure that does not demand internal reflection. If the Q-switch cell is some distance away from the mirror, then a pulse circulating in the cavity will "open" the Q-switch, i.e. modulate the cavity losses, twice for each cavity round-trip; once approaching the mirror and again leaving the mirror. Hence two pulses can be induced to circulate in the cavity, separated once again

by the round trip time between the dye cell and the mirror.

Clearly this process can repeat itself eventually generating a series of equally spaced sub-structure pulses. The number and intensity of these pulses should increase with the number of cavity cycles completed. In other words, the beginning of the pulse train should consist of single pico-second pulses with the fine structure appearing more in the later stages of the pulse train.

The T.P.F. pattern represents an average over all the pulses in the Q-switch envelope. In this description the convolution spots furthest from the mirror are due to pulses appearing only near the end of the pulse train and consequently give fainter integrated fluorescence. Malyutin (1972) on the basis of his work using time-resolved spectroscopy gives a similar description of the evolution of the structure of the pulse train.

CHAPTER V

CONCLUDING REMARKS

In the preceding chapters we have presented a full description of a pico-second laser facility. We can summarize the important operating characteristics as follows.

The free-running pulses have energies between 1 and 2 joules (and a beam divergence $\sim 10^{-4}$ radians). The emission consists of a millisecond burst of random spikes in the time domain with a spectrum consisting of several overlapping lines within a bandwidth of ~ 40Å.

The simultaneously Q-switched and mode-locked laser has a total energy output of about 200 millijoules per pulse. Each Q-switched output is seen to consist of a train of between 10 to 40 pico-second pulses (typically 5×10^{-12} sec long) having peak powers ~ 1 gigawatt.

The pulse trains last for about 100 nsec with the pulses separated by 7.5 nsec corresponding to the pulse circulation time of the cavity.

The individual pico-second pulses appeared to be followed by several satellite pulses of decreasing intensity separated by a space equal to twice the distance between the Q-cell and the adjacent mirror. These pulse groups are attributed either to multiple cavity lengths due to reflection from the interfaces within the Q-cell or (more probably) to the fact that the Q-switch is opened twice for each round trip of a

pulse circulating in the cavity.

It should be emphasized that the above parameters are not exactly repeatable. For example, the shape of the Q-switched pulse envelope and the number of pulses in a pulse train are not predictable but vary randomly from shot to shot.

One source of non-reproducible operation is thermal lensing. The wide variations in the threshold and output energies was shown to depend in a simple way on the pulse repetition rate. Further, it was found that single pulse trains were produced much more frequently when the laser was fired at a rate corresponding to a moderate amount of thermal lensing. It was concluded that thermal effects could be used to advantage in such applications rather than simply minimized (Ninnis and Rieckhoff, to be published).

Further investigations into mode-locking should include study of the generation of the aforementioned pulse groups. This investigation would be greatly aided by the capability of selecting a single pulse (or group) out of the train so as to study its individual fine structure. Understanding the connection between thermal lensing and the suppression of multiple pulse trains may be furthered by studying how the power spectrum and intensity correlation function of the laser output varies with the amount of thermal lensing.

APPENDIX A

TWO-PHOTON ABSORPTION

Two-photon absorption was predicted theoretically by Geoppert-Mayer in 1931 and confirmed experimentally by Kaiser and Garret in 1961. We present here a quantum mechanical description of two-photon absorption following closely the calculation of Yariv (1967).

The molecular system is assumed to be describable by a Hamiltonian H_0 have a set of energy eigenvalues E_n of the stationary states U_n, i.e.

$$H_0 u_n = E_n u_n \tag{A1}$$

The radiation field at frequency, ω, is introduced as a harmonic perturbation $H'(t)$ with matrix elements

$$H'_{km}(t) = \frac{H'_{km}}{2}\left(e^{i\omega t} + e^{-i\omega t}\right) \tag{A2}$$

We assume the system is in the ground state m at t = 0. Then second order time dependent perturbation theory gives the probability of finding the system in the state, ℓ, at time, t, as $|a_\ell^{(2)}(t)|^2$

$$\frac{d a_\ell^{(2)}}{dt} = \frac{-i}{\hbar} \sum_n a_n^{(1)} H'_{\ell n}(t) e^{-i\omega_{n\ell} t} \tag{A3}$$

And the first order coefficients $a_n^{(1)}$ are given by

$$\frac{da_n^{(1)}(t')}{dt'} = \frac{H'_{nm}}{2i\hbar}\left[\frac{1-e^{i(\omega-\omega_{mn})t'}}{i(\omega_{mn}-\omega)} + \frac{1-e^{-i(\omega_{mn}+\omega)t'}}{i(\omega_{mn}+\omega)}\right] \tag{A4}$$

Integration of (A4) and substitution into (A3) yields

$$\frac{da_\ell^{(2)}(t')}{dt'} = \frac{i}{4\hbar^2}\sum_n H'_{nm}H'_{\ell n}\left[\frac{1-e^{i(\omega-\omega_{nm})t'}}{\omega_{mn}-\omega} + \frac{1-e^{-i(\omega_{mn}+\omega)t'}}{\omega_{mn}+\omega}\right] \tag{A5}$$
$$\times\left(e^{i\omega t'} + e^{-i\omega t'}\right)e^{-i\omega_{n\ell}t'}.$$

In integrating (A5) we are interested only in those terms containing $\omega+\omega_{mn}$ in the denominator. These terms become dominant when $\omega=\omega_{mn}$ since $\omega>0$ and $\omega_{mn}<0$. The term of interest is thus

$$a_\ell^{(2)} = \frac{i}{4\hbar^2}H'_{nm}H'_{\ell n}\int_0^t \frac{1-e^{-i(\omega_{mn}+\omega)t'}}{\omega_{mn}+\omega}\, e^{-i\omega t'}\, e^{-i\omega_{n\ell}t'}\, dt' \tag{A6}$$

$$= \frac{1}{4\hbar^2}H'_{nm}H'_{\ell n}\left\{\frac{e^{i(\omega_{\ell n}-\omega)t}-1}{(\omega_{\ell n}-\omega)(\omega-\omega_{nm})} + \frac{e^{i(2\omega-\omega_{\ell m})t'}-1}{(2\omega-\omega_{\ell m})(\omega-\omega_{nm})}\right\}$$

using $2\omega-\omega_{nm}-\omega_{\ell n} = 2\omega-\omega_{\ell m}$.

The energy level diagram describing this process is shown in Fig. A-1.

Resonant absorption occurs when $2\omega = \omega_{\ell m}$ in which case the second term dominates and its squared magnitude is

$$\left|a_\ell^{(2)}(t)\right|^2 = \frac{\left|H'_{nm}H'_{\ell n}\right|^2}{16\hbar^4(\omega-\omega_{nm})^2}\,\frac{\sin^2\frac{1}{2}(2\omega-\omega_{\ell m})t}{\left[\frac{1}{2}(2\omega-\omega_{\ell m})\right]^2} \tag{A7}$$

Since levels ℓ and m are assumed to have some line-width we need to talk about the probability of finding the difference frequency $(2\omega-\omega_{\ell m})$. Writing $\rho(2\omega-\omega_{\ell m})$ as this normalized probability per unit ω, we find the probability of finding the system in state, ℓ, at time, t, to be

$$\underset{m\to\ell}{P(t)} = \frac{1}{16\hbar^4}\frac{|H'_{nm}H'_{\ell n}|^2}{(\omega-\omega_{nm})^2}\int_{-\infty}^{\infty}\frac{\sin^2(\frac{1}{2}xt)}{(x/2)^2}\rho(x)\,dx \qquad (A8)$$

$$= \frac{1}{8\hbar^4}\frac{|H'_{nm}H'_{\ell n}|^2}{(\omega-\omega_{nm})^2}\rho(2\omega-\omega_{\ell m})\pi t$$

using $x = 2\omega-\omega_{\ell m}$. This corresponds to a transition rate of

$$\underset{m\to\ell}{W} = \frac{dP(t)}{dt} = \frac{\pi}{8\hbar^4}\frac{|H'_{nm}H'_{\ell n}|^2}{(\omega-\omega_{nm})^2}\rho(2\omega-\omega_{\ell m}) \qquad (A9)$$

Now if the transitions are electric dipole, then the matrix elements H'_{nm} and $H'_{\ell n}$ are each proportional to the amplitude of the electric field, E, and so from equation (A9) we find $W \sim E^4$. This corresponds to an absorption which varies as the square of the intensity. Examination of equation (A9) also shows that the presence of a level, m, near the midpoint of the $m\to\ell$ transition greatly enhances the absorption probability. However, this condition implies a high optical density for the exciting radiation.

The best criterion for an atomic or molecular system to exhibit two-photon fluorescence is that the energy level separation between the ground state and the first excited

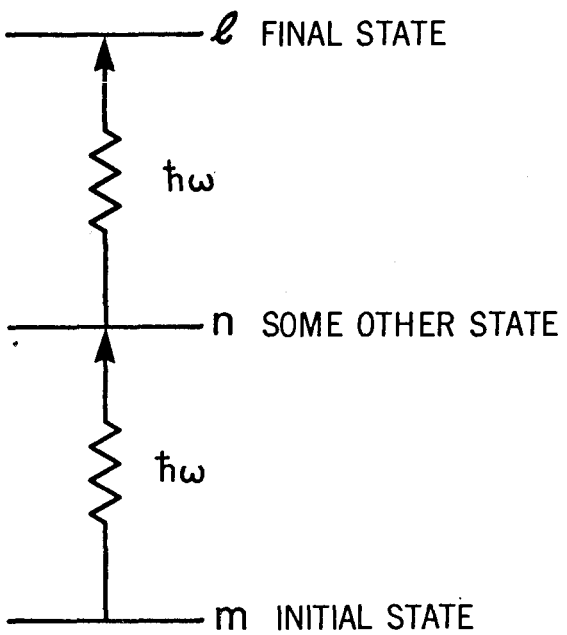

FIG A-1

REPRESENTATION OF TWO-PHOTON ABSORPTION

state be near (2ω) where ω is the frequency of the exciting light. In this case we may think of the simultaneous absorption of two photons by means of a virtual transition. It must also be remembered that two-photon absorption need not necessarily imply the corresponding single photon fluorescence since the selection rules (especially parity) may be different for the two processes.

If we assume a constant quantum efficiency for the absorption-fluorescence conversion, we have the important result that

$$ {}^{2\omega}I_f \sim {}^{\omega}I^2 $$

where ${}^{2\omega}I_f$ is the fluorescence intensity and ${}^{\omega}I$ is the intensity of the exciting radiation. This non-linearity is essential in the intensity correlation measurements.

APPENDIX B

RAY TRANSFER MATRIX FOR A BREWSTER-BREWSTER GEOMETRY

Suppose the ray transfer matrix (RTM) of an optical system having an index of refraction, n, and faces cut normal to the optic axis is

$$\begin{pmatrix} A & B \\ C & D \end{pmatrix}$$

The effect of replacing this system with one having end faces cut for Brewster-angle incidence will not be calculated. We start by finding the slope of an output ray relative to the optic axis, x′, in terms of the slope of the input ray. Fig. B-1(a) shows this situation for light rays leaving the medium.

Applying Snell's law to the ray shown

$$n \sin(\phi + x_0') = \sin(\gamma + x') \tag{B1}$$

or

$$n \sin\phi \cos x_0' + n \cos\phi \sin x_0' = \sin\gamma \cos x' + \cos\gamma \sin x'$$

This last equation can be solved for x′ by assuming the ray is paraxial keeping only first order terms in the expansion of sine and cosine and noting that

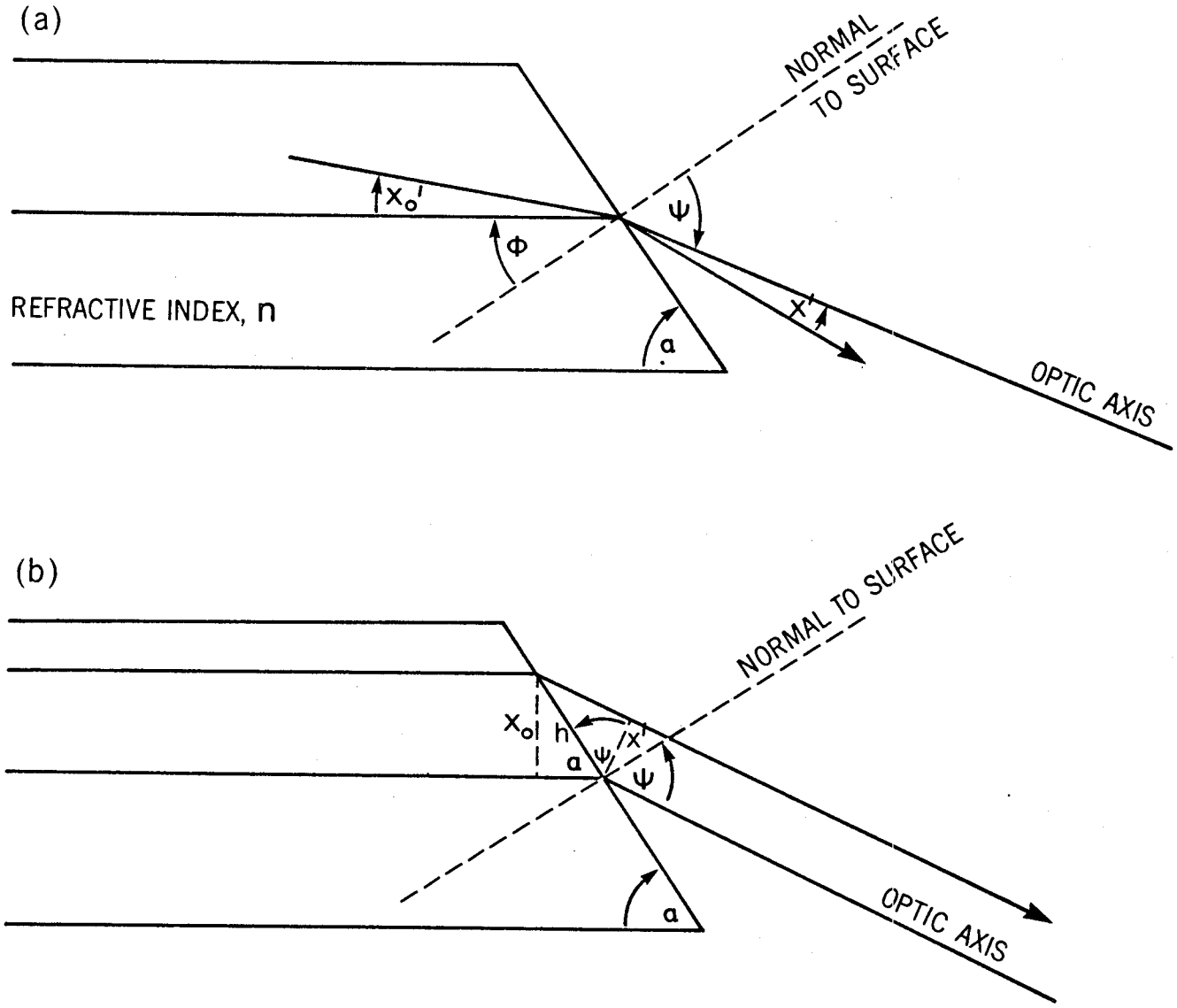

FIG B-1
GEOMETRY OF BREWSTER – CUT ROD

$$n \sin\phi = \sin\psi \qquad \text{(B2)}$$

The result is

$$x' = x_0' \frac{\cos\psi}{n\cos\phi} \qquad \text{(leaving the medium)}$$

and similarly (B3)

$$x' = x_0 \frac{n\cos\phi}{\cos\psi} \qquad \text{(entering the medium)}$$

It is clear from the geometry that

$$\phi + \alpha = \pi/2 \quad \text{, while} \quad \phi + \psi = \pi/2 \qquad \text{(B4)}$$

is the Brewster condition. It follows that $\psi = \alpha$ and $\phi = \pi/2-\alpha$ so that our result looks like

$$x' = \left(\frac{\cot\alpha}{n}\right) x_0' \qquad \text{(entering)}$$

and (B5)

$$x' = (n\tan\alpha)\, x_0' \qquad \text{(leaving)}$$

For the change in distance from the optic axis we assume

a ray parallel to the optic axis, thus neglecting the small dependence of x on x_0'. From Fig. B-1(b) we have

$$x_1 = h\cos\psi \qquad \text{and} \qquad x_0 = h\sin\alpha \tag{B6}$$

and using $\psi = \alpha$

$$x = (\tan\alpha)\, x_0 \qquad \text{(entering)}$$

and (B7)

$$x = (\cot\alpha)\, x_0 \qquad \text{(leaving)}.$$

Combining these results we have RTM's for entering and leaving the medium with Brewster-cut surfaces.

$$\begin{pmatrix} x \\ x' \end{pmatrix} = \begin{pmatrix} \tan\alpha & 0 \\ 0 & \frac{\cot\alpha}{n} \end{pmatrix} \begin{pmatrix} x_0 \\ x_0' \end{pmatrix} \qquad \text{(entering)}$$

(B8)

$$\begin{pmatrix} x \\ x' \end{pmatrix} = \begin{pmatrix} \cot\alpha & 0 \\ 0 & n\tan\alpha \end{pmatrix} \begin{pmatrix} x \\ x_0' \end{pmatrix} \qquad \text{(leaving)}$$

In order to find the RTM for the lens-like rod as a whole we simply multiply on the left by the matrix for each successive region.

$$\begin{pmatrix} Q & R \\ S & T \end{pmatrix} = \begin{pmatrix} \cot\alpha & 0 \\ 0 & n\tan\alpha \end{pmatrix} \begin{pmatrix} A & B \\ C & D \end{pmatrix} \begin{pmatrix} \tan\alpha & 0 \\ 0 & \frac{\cot\alpha}{n} \end{pmatrix}$$

(total effect) (leaving) (lens medium) (entering)

$$= \begin{pmatrix} A & \frac{B}{n^3} \\ n^3 C & D \end{pmatrix} \qquad \text{(B9)}$$

where we have used the Brewster condition, $\tan\alpha = n$.

LIST OF REFERENCES

Armstrong, J.A. 1967. Appl. Phys. Letters 10, 16.

Burnham, D.C. 1970. Appl. Opt. 7, 1727.

Bloembergen, N. 1965. Nonlinear Optics (New York: W.A. Benjamin, Inc.).

Brewer, R.G. and Rieckhoff, K.E. 1964. Phys. Rev. Letters 13, 334A.

Chiao, R.Y., Garmire, E., Townes, G.H. 1964. Quantum Electronics and Coherent Light, Proc. Int'l School of Physics, Enrico Fermi, Course XXXI, P.M. Miles and C.H. Townes, eds. (New York: Academic Press) pp 326-38.

Chun, M.K. and Bischoff, J.T. 1971. IEEE J. Q-E 7, 200.

Cutler, C.C. 1955. Proc. I.R.E. 43, 140.

DeMaria, A.J. 1966a. Appl. Phys. Letters 7, 174

DeMaria, A.J. 1968b. Electronics, Sept., 1968.

DeMaria, A.J., Glenn, W.H.Jr., Brienza, M.J., Mack, M.E. 1969c. Proc. IEEE 1, 2.

Fleck, J.A.Jr. 1969. J. Appl. Phys. 39, 3318.

Franken, P.A. and Ward, J.F. 1963. Rev. Mod. Phys. 35, 23.

Giordmaine, J.A. and Miller, R.C. 1965. Phys. Rev. Letters 14, 973.

Glen, W.H. and Brienza, M.J. 1967. Appl. Phys. Letters 10, 221.

Goeppert-Mayer, 1931. Ann. Physik. 9, 273.

Hargrove, L.E., Fork, R.L., Pollack, M.A. 1964. Appl. Phys. Letters 5, 45.

Hellwarth, R.W. 1961. Advances in Quantum Electronics, J.R. Singer, Ed. (New York: Columbia University Press) p. 334.

Javan, A., Bennett, W.R.Jr., Heriott, D.R. 1961. Phys. Rev. Letters 6, 106.

Kaiser, W. and Garrett, C.G.B. 1961. Phys. Rev. 7, 229.

Koechner, W. 1970. Appl. Optics 10, 2548.

Kogelnick, H. 1965. Bell Syst. Tech. J. 44, 495.

Lengyel, B.A. 1971. Lasers, second edition (New York: Wiley) p. 71.

McLung, F.J. and HelLwarth, R.W. 1962. J. Appl. Phys. 33, 828.

Maiman, T.H. 1960. Nature 187, 493.

Malyutin, 1972. Private communication.

Mann, M.M. and DeShazer, L.G. 1970. J. Appl. Phys. 7, 2951.

Osterink, L.M. and Foster, J.D. 1968. Appl. Phys. Letters 4, 128.

Picard, R.H. and Schweitzer, P. 1970. Phys. Rev. A 6, 1803.

Schawlow, A.L. and Townes, C.H. 1958. Phys. Rev. 112, 1940.

Shapiro, S.L. and Duguay, M.J. 1969. Phys. Lett. 28A, 698.

Snitzer, E. 1966. Appl. Optics 10, 1487.

Steele, E.L. 1968. Optical Lasers in Electronics (New York: Wiley).

Treacy, E.B. 1968. Phys. Lett. 28A, 34.

Voron'ko, O.N., Kozlov, N.A., Mak, A.A., Malinin, B.G. Stepanov, A.I. 1967. Sov. Phys. - Soklady 3, 252.

Weber, H.P. and Dändliker, R. 1968. IEEE J. Quant. Elect. 12, 1009.

Yariv, A. 1967. Quantum Electronics (New York: Wiley)